Beatriz Oliveira Esteves

Bachelor of Science in Materials Engineering

Perovskite solar cells: Optimization of Cost-Effective Production

Dissertation to obtain the Master Degree in

Materials Engineering

Supervisor: Dr. Manuel J. Mendes, Post-Doc Fellow and Invited Assistant Professor
Faculty of Sciences and Technology – New University of Lisbon

Co-Supervisors: Dr. Rodrigo Ferrão de Paiva Martins, Full Professor
Faculty of Sciences and Technology – New University of Lisbon
Dr. Shrabani Panigrahi, Pos-Doc Fellow
Faculty of Sciences and Technology – New University of Lisbon

Jury:

President:
Examiner: To be announced
Member:

FACULDADE DE CIÊNCIAS E TECNOLOGIA
UNIVERSIDADE NOVA DE LISBOA

September, 2018

Perovskite solar cells: Optimization of Cost-Effective Production

À minha família, em especial ao meu orgulho:

o meu irmão

Acknowledgements

Em primeiro lugar gostaria de agradecer ao Prof. Dr. Rodrigo Martins e à Prof. Drª Elvira Fortunato por me proporcionarem todas as condições necessárias para a realização desta dissertação, quer no CENIMAT como no CEMOP. Em especial atenção agradeço aos meus orientadores: Prof. Manuel Mendes, Prof. Dr. Rodrigo Martins e Shrabani Panigrahi, pela confiança depositada neste trabalho, pela oportunidade de investigar numa área tão cativante e com tanto impacto na sociedade atual bem como por todo o apoio e tempo despendido no decorrer deste projeto. *A special Thank you for my co-adviser, Shrabani Panigrahi, for all the good advices, the clarified questions, for all the time explaining me how to do and improve my devices and for all the depositions of gold.*

Não podia deixar de agradecer a toda a equipa do CENIMAT por toda a ajuda em certas etapas deste trabalho. Bem como aos ex-alunos que trabalharam neste tema, em especial ao Eduardo Duarte, por todo o trabalho deixado em mãos e por todas as dúvidas esclarecidas.

Não posso deixar de agradecer às pessoas que me auxiliaram a rever os erros existentes nesta tese. Nomeadamente ao Diogo, por todas as horas despendidas para melhoraria deste documento.

Não menos importante são as pessoas que me acompanharam durante estes 5 anos. São muitas as que um muito Obrigado não chega, um Obrigada por estes 5 anos intensos e acima de tudo (muito) felizes. Um Obrigada aos meus colegas de curso, sem especificar nenhum nome- vocês sabem quem são, sem vocês esta caminhada não seria igual. Um Obrigada por todas as gargalhadas e choros, por todas as brincadeiras, por todas as horas de estudo e por sempre me apoiarem antes e durante o decorrer deste projeto. Foram um apoio fundamental para que conseguisse chegar ao fim! Sem dúvida que vos vou guardar no meu coração, eternamente e com um carinho muito especial.

Não podia deixar de agradecer às amizades que fiz na TunaMaria. Obrigada pelas aventuras, pelos momentos, pelas melodias, pelas viagens, pelos sorrisos e até pelas lágrimas. Obrigada por me distraírem nos momentos mais frustrantes e por me apoiarem sempre. Sem vocês, este percurso, não era tão feliz!

Por fim, gostaria de agradecer às pessoas mais especiais da minha vida: a minha família, que tanto me orgulho. Sei que não foi fácil, mas Obrigada pais! Obrigada por me apoiarem sempre, mesmo longe o vosso apoio é insubstituível. Obrigada por me proporcionarem 5 anos de muito conhecimento! Um Obrigada aos meus avôs por toda a ajuda e carinho dado em todas as idas a casa. E um grande Obrigada ao meu irmão, por toda a confiança que me dá, por todas os "força mana, vais conseguir", por todas as mensagens sem sentido mas que fazem muita diferença e por todos os telefonemas atenciosos nos momentos mais difíceis na conclusão deste documento.

Um grande Obrigada a Todos!

Abstract

Solar energy exploitation via photovoltaic (PV) technology has become the main route to achieve sustainable development. The emerging perovskite-based PV is considered one of the most promising alternative technologies to the conventional Silicon solar cells, since perovskites are a class of semiconductor materials with quite favourable optoelectronic proprieties that allow attaining high sunlight-to-electricity conversion efficiency.

The main objective of this work is to improve the performance of perovskite solar cells (PSCs) using low-cost techniques and materials. Here, the perovskite ($CH_3NH_3PbI_3$) is produced as the active layer, Titania (TiO_2) and copper thiocyanate (CuSCN) are used as the electrons and holes transport layers, respectively. The production of homogeneous films is performed via spin-coating without atmospheric control, which is a great challenge in this area. In addition, the use of the inexpensive CuSCN hole transporter is developed, since it is 200 times less expensive than the conventionally-used Spiro-OMeTAD. This thesis was also investigated the crystallinity and quality of the perovskite film by a range of characterization tools such as XRD, SEM-EDS, AFM and UV-visible spectroscopy; as well as the influence of moisture on the active layer.

The optimization of the fabrication methods was performed successfully, as demonstrated by the achievement of perovskite films with an absorbance of approximately 90-95% and large grain sizes of 333 ± 94 nm, allowing a PSC efficiency of 6.35%, with V_{OC} of 0.89V, J_{SC} of 15.46 mA/cm^2, FF of 0.46, R_{SH} of 2516 Ω and R_S of 356 Ω.

Keywords: Photovoltaic technology, solution-processed perovskite solar cell, $MAPbI_3$, spin-coating, CuSCN, *J-V* curves

Resumo

A exploração da energia solar através da tecnologia fotovoltaica (PV) tornou-se o principal meio para alcançar o desenvolvimento sustentável. Uma alternativa às convencionais células solares de silício é a tecnologia PV baseada em perovskite, já que esta classe de materiais semicondutores oferece propriedades optoeletrônicas bastante favoráveis que permitem obter uma elevada eficiência de conversão de luz solar em eletricidade.

O principal objetivo deste trabalho é melhorar o desempenho das células solares de perovskite (PSCs) usando técnicas e materiais de baixo custo. Deste modo, a perovskite ($CH_3NH_3PbI_3$) é produzida como camada ativa, a titânia (TiO_2) e o tiocianato de cobre (CuSCN) assumem o papel de camada de transporte de eletrões e de buracos, respetivamente. A produção de filmes homogéneos é realizada via *spin-coating*, sem controle atmosférico o que se trata de um grande desafio nesta área. Além disso, foi desenvolvido o CuSCN como transportador de buracos, uma vez que este é 200 vezes mais barato que o convencionalmente usado Spiro-OMeTAD. Nesta tese também foi estudada a cristalinidade e a qualidade do filme de perovskite através de uma série de ferramentas de caraterização como XRD, SEM-EDS, AFM e espectroscopia UV-visível; bem como a influência da humidade na camada ativa.

A otimização dos métodos de fabricação foi realizada com sucesso, como demonstrado pela obtenção de filmes de perovskite com uma absorvância de aproximadamente 90-95% e tamanho de grão de 333 ± 94 nm, conferindo uma eficiência de 6.35%, V_{OC} de 0.89V, J_{SC} de 15.46 mA/cm^2, FF de 0.46, R_{SH} de 2516 Ω e R_S de 356 Ω.

Palavra-Chave: Tecnologia fotovoltaica, células solares de perovskite produzidas por solução, $MAPbI_3$, spin-coating, CuSCN, Curvas *J-V*

Abbreviation

ABX_3 - $CH_3NH_3PbI_3$ or $MAPbI_3$ - Methylammonium Lead Iodide

AFM -Atomic force microscopy

CAS - Chemical Abstracts Service

CB - Conduction band

c:TiO_2 – compact TiO_2

CIGS - Copper indium gallium selenide

DMF - N,N-dimethylformamide

DMSO - Dimethyl Sulfoxide

EDS - Energy Dispersive Spectroscopy

ETL - Electron transport layer

ETM - Electron transport material

EtOH - Absolute Ethanol

FF - Fill factor

FTO - Fluorine-doped Tin Oxide

HTL - Hole transport layer

HTM - Hole transport material

ITO - Indium tin oxide

J_{SC} - Short-Circuit Current Density

Li-TFSI - Bis(trifluoromethane) sulfonimide – Lithium salt

MAI - Methylammonium Iodide

mp:TiO_2 - mesoporous TiO_2

PCE - Power Conversion Efficiency

PSC - Perovskite solar cell

PTTA - Poly[bis(4-phenyl)(2,4,6-trimethylphenyl)amine]

PV - Photovoltaic

R_S - Series resistance

R_{SH} - Shutt resistance

RT - Room temperature

SC - Solar cell

SEM - Scanning electron microscopy

Spiro-MeOTAD - 2,2’,7,7’-tetrakis(N,N-di-p-meth-oxyphenylamine)-9’,9’-spirobifluorene

TCO - Transparent conducting oxide

TTIP – Titanium (IV) isopropoxide

UV - Ultraviolet

VB - Valence band

V_{OC} - Open-circuit voltage

XRD - X-ray diffraction

FIB - Focused ion beam

I_{SC} - Short-Circuit Current

Symbols

µL - Microliter

Å - Ångström

Al_2O_3 - Aluminum oxide

Au - Gold

CdTe - Cadmium telluride

cm - Centimeter

c-Si - Crystalline silicon

CuI - Copper iodide

CuSCN - Copper(I) Thiocyanate

GaAs - Gallium arsenide

HCl - Hydrogen chloride

kHz - Kilohertz

Li - Litium

mA - Microamperes

mg - Miligrame

min - Minute

mL - Milliliter

mm - Millimeter

N/m - Newton metre

NiO - Nickel oxide

nm - Nanometer

ºC - Degrees Celsius

Pb - Lead

PbI_2 - Lead iodide

rpm - Rotations per minute

s - Seconds

TiO_2 - Titania or Titanium dioxide

V - Voltage

ZnO - Zinc oxide

ZrO - Zirconium Oxide

λ - Wavelength

Ω - Ohms

Ω/sq - Ohms Per Square

List of Contents

List of Figures

List of Tables

Motivation and Objectives

Solar energy has a key role in ensuring a sustainable development since it has the least impact in the environment. In addition to this, the sunlight is one of the most cleaned energy sources which contributes to this sustainability.

Over the years, silicon-based cells have been used for industrial purposes due to their achieving efficiencies of 26%, especially crystalline silicon [1]. However, silicon-based photovoltaics cells are a high expense of critical processing techniques as it requires high temperature or vacuum [2]. Meanwhile, the technology based on thin films and simple deposition methods promise low production cost and semiconductor with high quality.

A new class of thin film SCs which has drawn considerable attention and interest to the scientific community is the perovskite SCs. They were introduced to literature in 2009 with a low power conversion of only 3.8% [3]. The interest in this SCs was triggered in 2012 when got 9,7% with a stability of 500h [4]. This type of SCs has a great efficiency compared to the existing organic and dye-sensitized solar cells, reaching top position (22,7%) in 2017. This result arises from its high charge mobility, broadband absorption [5], substantial improvement Power Conversion Efficiency (PCE).

The aim of this work is to improve the performance of perovskite solar cells using TiO_2 as Electron Transport Layer (ETL), $CH_3NH_3PbI_3$ as an active layer and CuSCN as Hole Transport Layer (HTL). Besides, to get a better understanding of the important factors on the SC's fabrication using low cost, simple and fast production methods. In order to do that, the influence of different parameters was studied, as described below:

- ETL and HTL fabrication, using different conventional solutions for TiO_2; the influence of planar and mesoporous architecture; the impact of Li^+ doping; using different solvents in CuSCN as di-n-propyl sulfide and dipropyl sulfide and the influence of filtering this solution and its amount deposited. The importance of these changes on the solar cell's performance as well as transmittance and reflectance spectrum analysis were conducted.
- Perovskite layer fabrication and optimization: different ways to anneal (hotplate and tube furnace), the influence of filtering the perovskite solution and loading time of perovskite. To observe the effect of these changes on the SC's performance, SEM images, EDS, XRD and absorbance spectrum analysis were performed.
- Solar cells fabrication and characterization. Using a Sun Simulator, the photovoltaic response was obtained, and the main solar cells parameters were calculated. XRD and absorbance spectrum were completed to characterize the solar cell structure morphology and composition, while the layer thicknesses were measured by cross-section SEM image.

1 Introduction

In the last decades, solar energy has been playing an important role to ensure a sustainable development due to being an alternative source to traditional resources such as coal and fossil fuels. Recent studies indicate that this will account for 35% of global electricity generation capacity by 2040 [6]. In perspective, solar cell (SC) optimization is one of the best approaches for the development and conversion of solar energy (electromagnetic radiation) into electric energy based of photovoltaic effect (PV).

Light absorption, charge separation, charge transport, and charge collection are fundamental for photovoltaic process (Figure 1) [4]. In the conversion process, the incident light with energy equal to or higher than the band gap creates electron-hole pair into free electric charges which are separated within the device by the electric field of the junction, producing an external electric current (*I-V curve*).

Solar cells are divided in three generations according to their stages of development. The first generation of solar cells is made of silicon crystal. Crystalline silicon SCs are present in 90% of commercial photovoltaic devices [7]. The second generation of SCs consists of thin films materials, such as CdTe, CIGS or GaAs [4]. Many of these materials are too expensive (GaAs), too toxic (CdTe) [8], rare or don't allow low fabrication temperatures. The third generation, another thin film technology consists of organic, dye-sensitized, polymer and perovskite solar cells [9], [10].

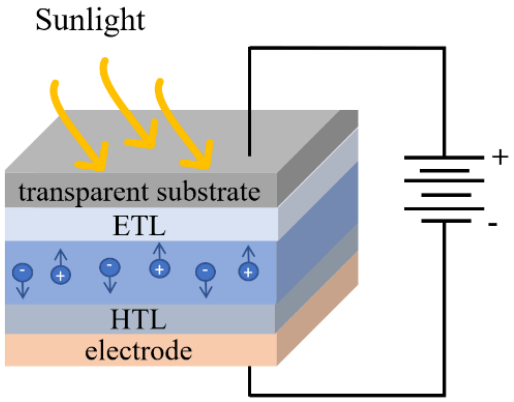

Figure 1 | A solar cell: basic device for solar energy conversion.

1.1 Perovskite Solar cell

1.1.1 Crystal structure

Perovskites have the common chemical formula ABX_3, whose structure and physical properties were first described by Weber in 1978 [4]. A and B are cations which reside in the corner and the body centre of the pseudocubic unit cell and X is the anion which occupies the face centre (Figure 2) [11]. The larger cation A is considered organic, which is generally methylammonium ($CH_3NH_3^+$ or MA). Ethylammonium and formamidinium (FA) also offer

excellent results. The anion X is a halogen, normally iodide (I^-), Br^- and Cl^- are also used in perovskites as well as mixed halide materials. For cation B, Pb is universally considered for stabilization and efficiency in solar cells although Sn^{2+} and Ge^{2+} can also be used due to being in the same group as Pb^{2+}. Their performance is poor compared to Pb efficiency [11], [12]. It should be noted that cation A is the most important component of the perovskite molecule, determining the structure and the crystal size. Thus, it influences directly the perovskite's stability and its optoelectronic properties [7].

The crystalline structure of perovskite can grow in the cubic, tetragonal or orthorhombic phases depending on annealing temperature [13]. The symmetry of the perovskite is proportional with an increase of the temperature: $CH_3NH_3PbI_3$ ($MAPbI_3$) exhibits the orthorhombic phase below room temperature (RT), and from RT it is observed a tetragonal configuration [9].

1.1.2 Perovskite properties

The materials of the perovskite family present multiple electronic properties, including thermoelectric, piezoelectric, superconductivity and semiconductivity, depending on the type of material considered. [9]. The $MAPbI_3$ exhibits unique features such as strong absorption over the visible and near-infrared spectra [7],[14], uplifted mobilities and diffusion lengths in the µm range [7], lower surface recombination rate [9] appropriate band gap (1,4 – 2,2 eV [15]) and solution processability [16]. Despite these favourable properties, PSCs have negative aspects such as photocurrent hysteresis [17] and some problems of toxicity, due to lead being the major constituent of all high performing of PSCs to date, thus raising issues during device's fabrication, deployment and disposal [14], [18].

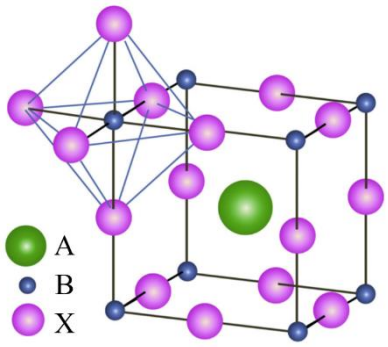

Figure 2 | Crystal structure of organic-inorganic halide perovskites ABX_3 ($MAPbI_3$) [8]

Another critical disadvantage of PSCs is their sensitivity to moisture, both during processing and their useful lifetime [19]. This degradation can occur essentially because MA cation has a weak connection via hydrogen bonds with lead and iodide. Therefore, a water molecule can break these bonds or even a low moisture content can result in the decomposition of PbI_2 [20]. However, there have been several debates about it. When the perovskite is exposed to very low levels of moisture, it is possible to be beneficial. On the other hand, long term contact to air is harmful to SCs performance.[21] Most scientific articles states that PSCs are manufactured under highly controlled atmospheric conditions, typically with a glove box, in order to maintain acceptable

atmospheric conditions and achieve high performance. The capacity to produce devices at a non-controllable atmospheric humidity represents a step forward for the eventual commercialization [19].

1.1.3 Perovskite film preparation

Fabricating perovskite films with better quality is of crucial importance in order to achieve superior efficiencies. To obtain good optoelectronic properties in perovskite films, it is necessary to have a control of the crystallinity which is related to the morphological development. Furthermore, morphology has influence on the charge dissociation, diffusion lengths and charge recombination dynamics in the resulting perovskite layer [22]. The morphological characteristics depend on some important factors, such as the method of perovskite deposition on the substrate, annealing temperature, duration for which temperature is maintained, atmospheric conditions during film growth, initial material proportion and solvents/additives used [9]. The perovskite layer is expected to possess efficient surface coverage and large grain size to obtain high performance[23]. In contrast, inhomogeneous perovskite layer leads to pinhole formation and incomplete surface coverage, resulting in increased shunting paths and inefficient light absorption in devices [24]. In order to dominate the described challenges, researchers have introduced some scientific techniques, from hot-casting [25], solvent engineering [26] to anti-solvent [27]. These methods are based on two points of view, inducing rapid homogenous nucleation followed by growth of crystalline perovskite (hot casting and antisolvent methods), and changes in the intermediate phases delays the crystallization of perovskite (solvent engineering) [28]. In adition, various methods for PSCs fabrication techniques have been reported such as spin-coating (used in this work), spray coating, inkjet printing, vacuum sublimation, doctor blade printing and slot-die coating methods [16].

a. Spin coating

Spin-coating, one of the most economical film production methods, is widely used in PSC processed by solution [26]. In this case, it is important to adjust some parameters such as temperature, solution wettability and viscosity, spinning rate and time [4]. In addition, by following this method, it is possible to achieve better morphology while simultaneously being simple, cost-effective and environmentally conscious [24]. However, it requires a controlled procedure. The anti-solvent (like toluene, diethyl ether or chlorobenzene [19]) induces excessive saturation of the perovskite solution and it is generally dripped into the centre of the film during spin-coating. Thus, it results in a radial supersaturation gradient and, consequently, a spatially inhomogeneous nucleation of the perovskite layer, leading to defects in the film [29]. Besides that, the evaporation during spinning immediately induces the formation of well-crystallized perovskite materials due to the strong ionic interaction between metal cations and halogen anions [26].

1.1.4 Perovskite solar cell architecture

The general layer structure for PSCs contains a transparent conductive oxide – typically Fluorine-doped Tin Oxide (FTO) or Indium Tin Oxide (ITO) – over a glass substrate, an electron transport layer (ETL), an active material (perovskite), a hole transport layer and lastly a metallic electrode. The metallic layer and TCO work as a conducting electrode, while HTL and ETL serve as an interfacial modifier. The perovskite material acts as a light absorber and transports the charge till their arrival at the respective electrodes [9]. The metal electrodes are usually made of gold for better bonding with the other layers, although other non-precious metals have also been explored (nickel, aluminium or silver) [30].

In some cases, there are variations in the regular structure of PSCs, some of which were considered free of ETM (and HTM) and PSCs only free of HTM [6]. Moreover, two main architectures are commonly used for PSCs: planar (Figure 3 a)) and mesoscopic (Figure 3 b)). Furthermore, the so-called inverted device structure (Figure 3c)) designates an architecture in which each layer is fabricated in the reverse order of the "normal" assembly, and thereby the device is illuminated through the HTM layer. [31].

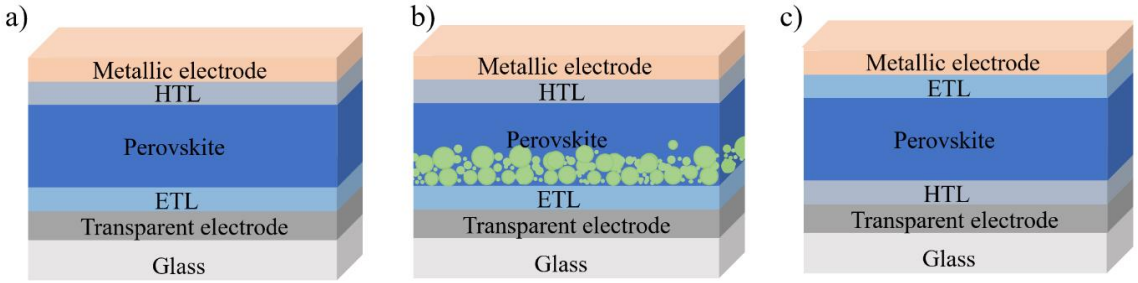

Figure 3 | Schematics illustration of perovskite solar cells in a) planar, b) mesoscopic and c) inverted architectures [9].

a. Electron and hole transport material

For PSCs to function properly, the energy levels of each material layer need to be carefully planned. This way, to realize an efficient hole and electron transport and extraction, it is important to have a valence band (VB) of HTMs higher than VB of perovskite materials and a conduction band (CB) of ETMs lower than CB of perovskite materials [24]. Figure 4 shows the diagram of the energy levels of the PSC device: FTO / TiO_2 / $CH_3NH_3PbI_3$ / CuSCN / Au and their respective generation and transport of charges. Based on perovskite and energy level alignment, the electrons can be transferred to the conduction band of TiO_2, and the holes can be collected by HTM (CuSCN), then passed to the counter electrode.

The ETL is a key component of the PSCs and must provide efficient extraction and collection of electrons, minimizing charge recombination at interfaces to ensure high performance [32]. There are some electron transport materials (ETMs) such as ZnO, ZrO and TiO_2 [15]. The previous being the most used (in compact and mesoporous architecture) due to being transparent to visible light, having low absorption and high refractive indices [6]. However, the electron mobility of TiO_2 is much lower than the electron mobility in the perovskite layer and the electron

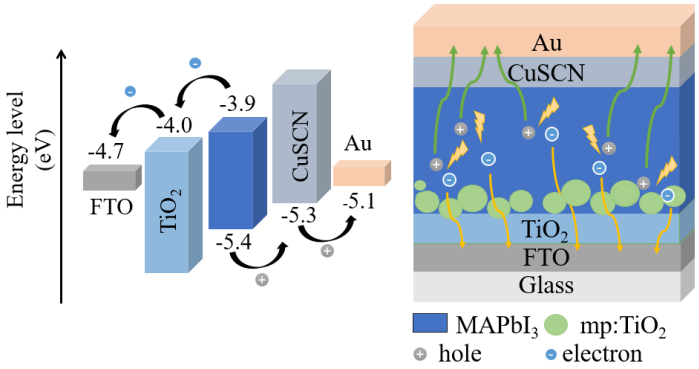

Figure 4 | a) Energy level diagram of each material layer considered in this work b) scmatics of PSC with mesopouros layer. Charge generattion and transport process are illustrated. Adapted from [3], [11], [58] .

transport length in the mesoporous layer is higher than in the compact layer of TiO_2 [33]. The disadvantage of TiO_2 is that a high processing temperature (> 400 °C) is required, which results in the impossibility of using low-cost, lightweight and flexible plastic substrates because they are unstable at high temperatures [34]. Furthermore, using a mesoporous TiO_2 layer (mp:TiO_2) enhances the performance of the photovoltaic devices as it increases the electron injection rate and the charge carrier lifetime and retards the electron–hole recombination [35],[36]. It was also demonstrated that mp:TiO_2 can be n-doped in a facile and effective way by a similar lithium salt surface treatment, facilitating electron injection and transport in the mp:TiO_2 [37].

The main function of HTL is to prevent direct contact between the perovskite and the metallic contact, which minimizes charge recombination and prevents degradation at the metal-perovskite interface either to extract perovskite positive charges (holes) and to transport them to the upper electrode [7]. The most common material used for the HTL layer is the Spiro-OMeTAD, which is very expensive [3]. Other organic and inorganic materials such as PTTA, CuI, NiO, CuSCN are also employed [15]. However, the cost of these organic HTMs is high for large scale applications and most of the solvents used for this layer have high solubility with the perovskite layer which causes their degradation [38].

Inorganic HTMs are a class of compounds with potentially greater stability than organic HTMs. From the inorganic materials examined to date, CuI, CuSCN and NiO exhibit the most promising performances with 7.5, 18.0 and 14.9% of PCE reported, respectively [20]. Regarding CuSCN, it is an abundant and a p-type semiconductor with high hole mobility, good thermal stability and a well-aligned working function. It is doped intrinsically and transmits light through the spectral region of visible and near-infrared [24]. In addition, it can be deposited by processing in solution at low temperature, making it compatible with flexible substrates [39].

2 Experimental

2.1 Device Fabrication

The following sections describe the perovskite solar cells' manufacturing process performed during this work. Fabrication of PSC is divided by etching FTO, cleaning the glass followed by deposition of: ETM, active layer, HTM and gold contacts. All the depositions, except the last one, were carried by spin-coating. The material information used in this work is presented in Table 12 from section B of Appendices. All the processes were done without a glove box and therefore there is no control of moisture.

2.1.1 Substrate preparation and ETL deposition

The fluorine-doped tin oxide (FTO) coated glass substrates (100 x 100 x 2.2 mm^3), with 25 Ω/sq and 80-85% of transmittance, cut into 2.5 x 2.5 cm^2, were selectively etched with Zinc powder and HCl with a cotton stick. After that, the FTO substrates were cleaned in an ultrasonic bath with detergent, water, acetone, isopropyl alcohol and ethanol in this order, for 15 min each. Then the substrates were dried with nitrogen flow and further cleaned with ultraviolet ozone treatment with temperature (80ºC) for 15 min to eliminate any organic contaminants and moisture.

For the ETL, two precursors were studied for the compact TiO_2 layer (c:TiO_2), detailed in section C.1 from Appendices. 150 µL were dropped in the subtract and spun at 4000 rpm (TiO_2 (1)) and 3000 rpm (TiO_2 (2)) for 35 s [33], respectively. After the spin-coating, the c:TiO_2 were dried at 120 °C for 10 min and then annealed at 500 °C, for 30 min and left to cool down to RT. Subsequently, a mesoporous TiO_2 layer (mp:TiO_2) was deposited, dropping 150 µL and spinning for 20 s at 4000 rpm, using a 150 mg/mL solution of 30 NRD TiO_2 paste (Dyesol) in EtOH, dried at 100 ºC for 10 min and then sintered at 450 °C for 30 min and left to cool down to RT.

For Li^+ treatment of the mesoporous TiO_2 scaffold, a 150 µL of LI-TFSI solution in acetonitrile (10mg/mL) was spin coated at 3000 rpm for 20 s after 10 s loading time, followed by another sintering step at 450 °C for 30 min and left to cool down to RT.

2.1.2 Perovskite precursor solution and film preparation

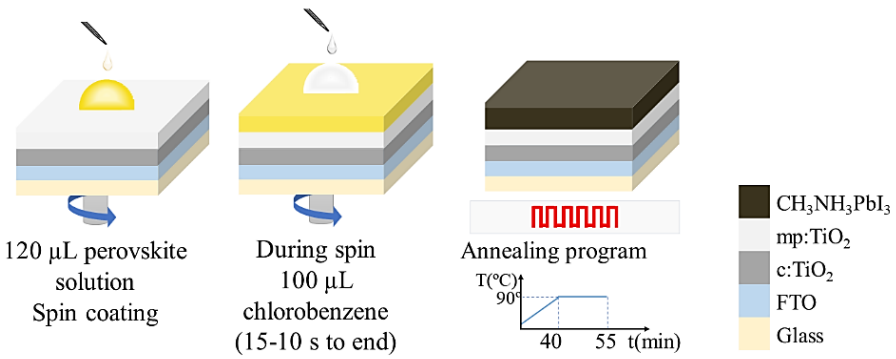

Figure 5 | Schematic illustration of perovskite deposition with a two-steps program.

To deposit perovskite solution (described in section C.2 from Appendices), the solution was filtered through a 0.2 µm syringe filter before used. Then 120 µL of solution was spin coated in a two-steps program at 1000 and 6000 rpm for 10 and 20 s respectively, with 30 s of loading time. During the second step, 100 µL of chlorobenzene were poured on the spinning substrate 10 s prior to the end of the program. The perovskite layers were annealed using an annealing program from RT to 90 ºC for 40 min and remained 15 min in a tube furnace with nitrogen flow. During the deposition it is important to keep the solution in the hot plate with stirring so the temperature does not decrease.

2.1.3Hole transporting layer and top electrode

After the perovskite annealing, the substrates were cooled down for few minutes. Two solutions were used and are described in section C.3 from Appendices. For first and second solutions,120 µL of filtered solution were droped, and spun at 4000 rpm for 30 s with no post heat treatment applied. Finally, using acetate masks fabricated by LASER (Universal LASER Systems), the counter electrode was deposited by electron-beam evaporation under a high vacuum with a thickness between 60-80 nm and an active area of 0.07 cm^2.

2.2 Characterization

2.2.1 SEM-EDS

The top-surface and cross-sectional images were examined by scanning electron microscopy (SEM) using a Carl Zeiss Auriga crossbeam (SEM-FIB) workstation instrument equipped with an Oxfotd Intruments Aztec X-ray energy dispersive spectrometer.

2.2.2 AFM

The atomic force microscopy (AFM) measurements were performed in an Asylum Research MFP-3D Standalone operated in alternate contact mode in air (commonly known as tapping mode), using commercially available silicon AFM probes (Olympus AC160TS; k = 26 N/m, f_0=300 kHz). The resulting topography were plane fitted in Igor Pro software (Wavemetrics) and the final images generated using Gwyddion software.

2.2.3 XRD

The crystal structures of the thin films were characterized with X-ray diffraction (XRD) by using a PANalytical X'Pert Pro X-ray diffractometer in Bragg-Brentano geometry, with a monochromatic Cu-Kα (λ=1.5406 Å).

2.2.4 UV-Visible Spectroscopy

The ultraviolet–visible (UV–vis) absorption was measured by a UV–vis Spectrophotometer Shimadzu UV 3101PC by obtaining reflectance and total transmittance with a ISR-260 integrating sphere within a range of 300-830 nm.

2.2.5 Electrical Characterization

The *J-V* curves were measured by SS150 Reflective Solar simulator from Sciencetech by forward scan (I_{SC} to V_{OC}) under ambient conditions at RT and AM1.5G illumination conditions (100 mW/cm^2). The SCs were characterized without encapsulating the devices.

3 Results and Discussion

As discussed in the introduction, in order to obtain an efficient perovskite solar cell, it is necessary to study and optimize its structure and morphology, although other layers may be studied to understand the influence of which one in SC operation. Therefore, this chapter is divided into ETL and HTL characterization; perovskite layer characterization and optimizing perovskite solar cells and humidity influence. The main characterization realized was electrical proprieties once the aim of this project is to increase the PSC performance. Nevertheless, other characterizations were made, including morphological, structural and optical.

3.1 ETL and HTL Optical Characterization

In this section, HTL and ETL are optically characterized to understand its contribution in SC performance. ETL must have a high transmittance to enable the light going through and to achieve the active layer. HTL is intended to absorb little radiation to avoid wasting any light which may not be absorbed by perovskite and that can be reflected by the gold. Therefore, this light would be absorbed again by the active layer.

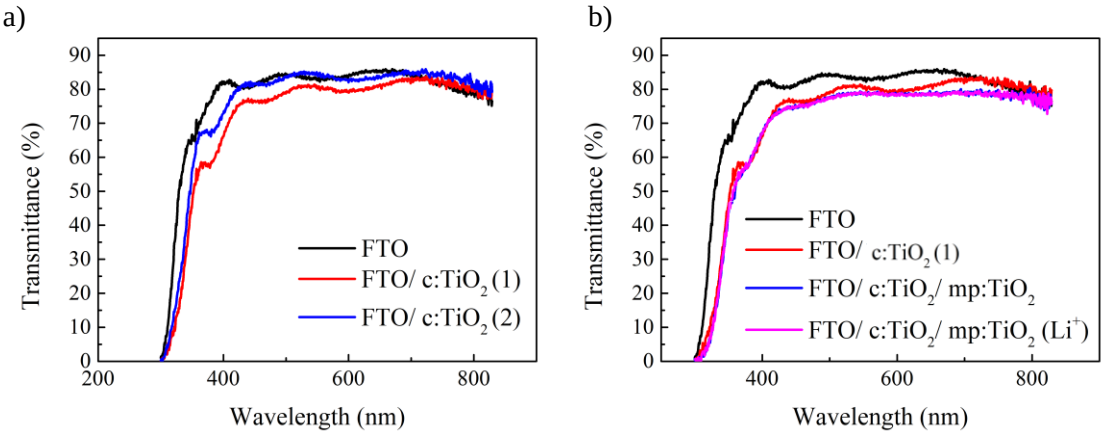

Figure 6 | Transmittance spectra of differents substracts as ETL over FTO (black), a) c:TiO2 (1) and (2) with red and blue, respectively and b) c:TiO2 (red), adding m:TiO2 (blue) and m:TiO2 doped with Li (pink) deposited with the final defined conditions for solar cells fabrication as described in section Experiemtal.

As said in the experimental section, two different TiO_2 solutions were prepared. In this section, it is called TiO_2 (1) for TTIP solution and TiO_2 (2) for Acetylacetone solution. Figure 6 a) and b) show the direct transmittance for the different TiO_2 deposited over FTO coated glasses and the transmittance spectra with the addition of compact, mesoporous TiO_2 and Li^+ treatment over FTO deposited coated glasses, respectively. The substrate made with c:TiO_2 (1) shows a lower transmittance compared with FTO and c:TiO_2 (2) due to its higher reflective index relative to FTO (n=1.8 - 2.0 for FTO and n=2.3 for TiO_2 [40]), as it is possible to see by the curves. Despite c:TiO_2 (2) being better optically for solar cell due to its higher transmittance and small reflectance,

it will not be used for ETL since when it is applied for the fabrication of solar cells this does not present favourable performances (Table 2 from section 3.2.2 of Results and Discussion).

Figure 6 b) shows that transmittance decrease with the addition of m:TiO_2, as expected, since with the deposition of this layer it is possible to observe an opaque film. However, it remains approximately constant if it is doped with Li^+. In addition, the transmittance's average reaches values of 82% which is remarkable since the transmittance remains high even with the addition of other layers over the glass. Further ahead it will be tested the influence of m:TiO_2 and Li^+ doped m:TiO_2 in solar cells performance, an increase of efficiencies is expected. [37]. All samples reached a maximum transmittance close to 90 % and low parasitic absorption (close to 10 % over FTO coated glass) in the UV-Vis spectrum, which is desired, specifically for ETL layers since, before reaching the active layer, the light will pass through the glass FTO-ETL (Figure 37 from section D of Appendices).

Although CuSCN is not used over FTO coated glass it is important to study this layer optically. Figure 7 a,b) shows the transmittance spectra for CuSCN made with different solutions. It is called CuSCN (1) for CuSCN dissolved in di-n-propyl sulfide and CuSCN (2) for the one dissolved in diethyl sulfide. No difference in absorbance can be observed for this two films, however, CuSCN (2) may be a better option since it has a low absorbance (i.e. high transmittance) and it is essential to avoid overlap with the parasitical absorption of $MAPbI_3$ [41]. The average of transmittance is 85% and the absorbance reaches values between 5-10% which is notable.

In these cases, it is not possible to rigorously determine the band gap since the films are too thin, making the absorbance spectrum behaviour to be mainly dominated by the glass. Thus, it was assumed the theoretical band gaps of 3.8 eV for TiO_2, 3.3 eV for CuSCN.

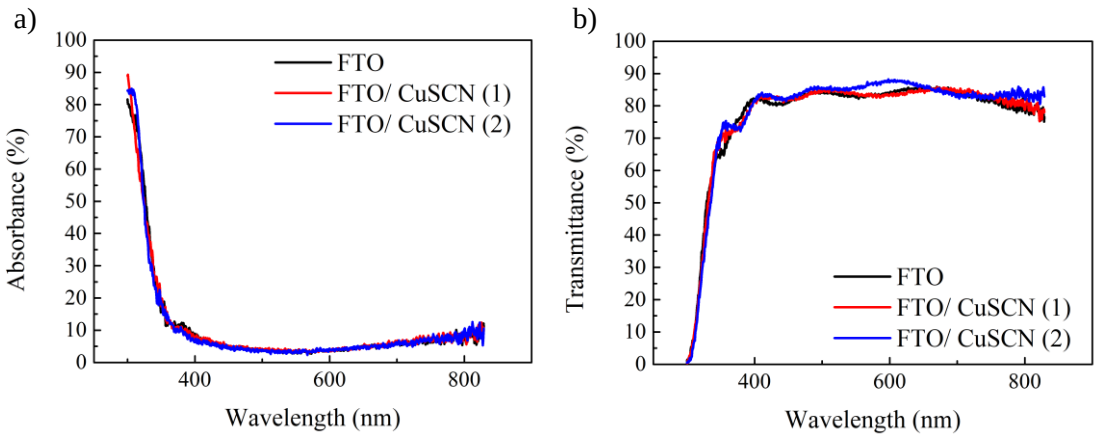

Figure 7 | a) Absorbance and b) Transmittance spectra of differents subtract as HTL: CuSCN (1) and (2) is CuSCN dissolved in di-n-propyl sulfide (red) and in diethyl sulfide (blue), respectively. CuSCN layer deposited as described in section Experiemtal.

3.2 Optimization of Perovskite Solar cell

For this section, techniques based in last works were used [42],[43] and the performance of PSCs was improved. Therefore, it is presented results of some SCs done in this work by chronological order. The batch fabricated has on average 8 samples, each of them have 8 contacts, usually. The *J-V* and *P-V* curve showed the best contact result of SC.

In this section the optical and the structural characterization are presented to understand the contributions of which parameter on the performances of PSC. Throughout this thesis, it was possible to verify the improvement of the PSC quality as we were unable to get a complete work batch in the beginning. The relative humidity was registered for the whole batch and in the section 3.3 of Results and Discussion, the relation between the obtained results (PCE and PSCs functioning) and moisture's influence will be analysed.

3.2.1 Hot plate vs tube furnace annealing

In the last works already mentioned above, the hot plate was used to anneal perovskite with the lower part of the sample directly contacting the surface of the plate and the other side of the sample being directly exposed to the air. Therefore, the entire system (sample and air environment) is not uniform in temperature. It is important to consider that the annealing method is a relevant factor that may be altered to control the quality of the perovskite layer.

In this study, PbI_2 + $3CH_3NH_3I$ precursor films on TiO_2/FTO/glass substrates were annealed both on hot plate and in a tube furnace (Figure 8). Moreover, in this case the tubular furnace is filled by a well-controlled temperature and it has nitrogen flow that makes an inert atmosphere. Figure 9 shows some visual differences between samples after annealing in a hot plate and tube furnace. It is possible to see some differences in colour and brightness of the SC.

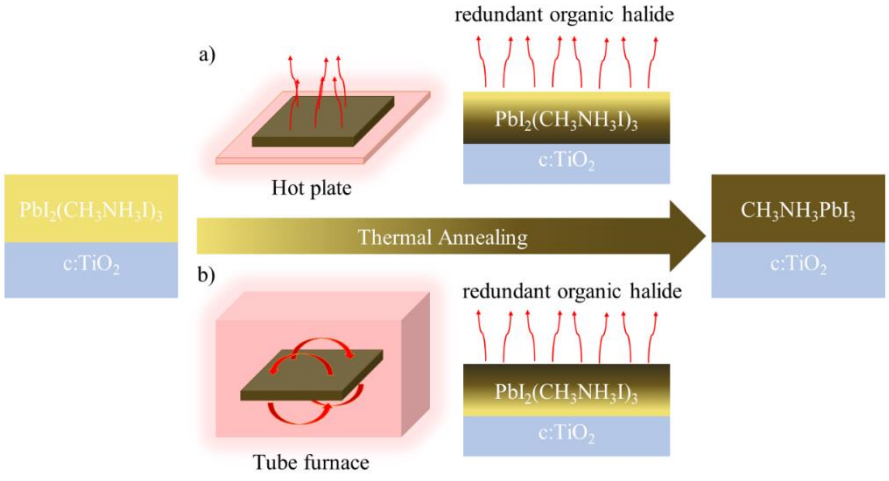

Figure 8 | Schematic of the annealing approaches. (a) hot plate. (b) tube furnace. Adapted by [44]

Regarding the absorbance spectra (Abs = 100% - T_{Total} - R_{Total}) in Figure 10 a), no significant differences are shown. Both samples demonstrate a variation of absorbance that reaches values between 87-93%. It is also possible to observe that perovskite has a band gap close to 1.52 eV which is expected [3],[15]. Band gap was obtained by fitting curves on the drop zone.

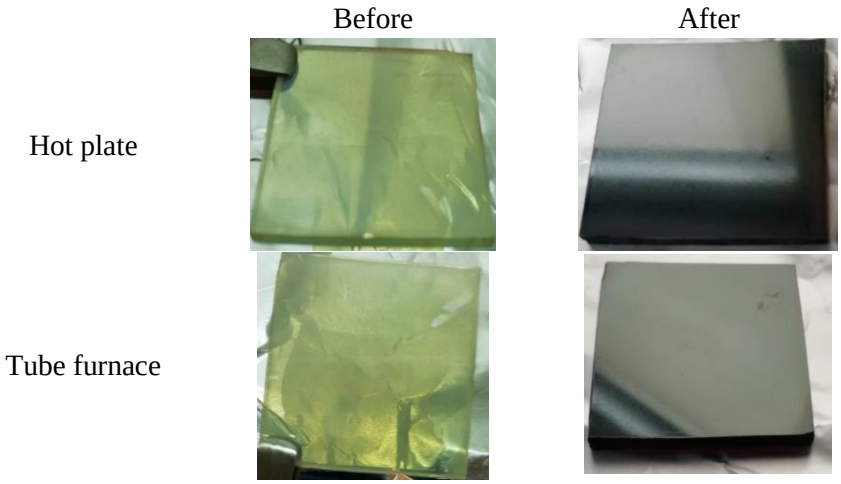

Figure 9 | Images of the samples annealed at hotplate vs tube furnace. Films were deposit over c:TiO_2 using TTIP precursor solution. Anneal in hotplate was done for 15 at 90ºC and tube furnace was an annealing program at RT to 90 ºC for 40 min and remaining 15 min.

The devices were also characterized using XRD (Figure 10 b)) where the results reveal, for both cases, the presence of (110), (112),(211), (202),(220), (310), (224) ,(314) planes at an angle 2θ of 14,1º, 20º, 23.52º, 24.5º, 28.5º, 31.87º, 40.55º, 43.17º respectively which indicate the tetragonal phase of $MAPbI_3$ marked with a full circle [45],[46],[47]. On the other hand, the peaks corresponding to the PbI2 phase, at 12.67° and 38.7º are marked with an empty circle [48]. In addition, the diffraction peaks of FTO at 26.52 and 37.75 are assigned to the (222) and (200) lattice planes, respectively [45] and are marked with a cardinal. These spectra demonstrate a higher PbI_2 peak for the perovskite fabricated using the tube furnace, indicating higher degree of organic degradation on the perovskite film. In contrast, it is observed that perovskite film is more crystalline when annealed in a tube furnace since the peaks of $MAPbI_3$ are more intense.

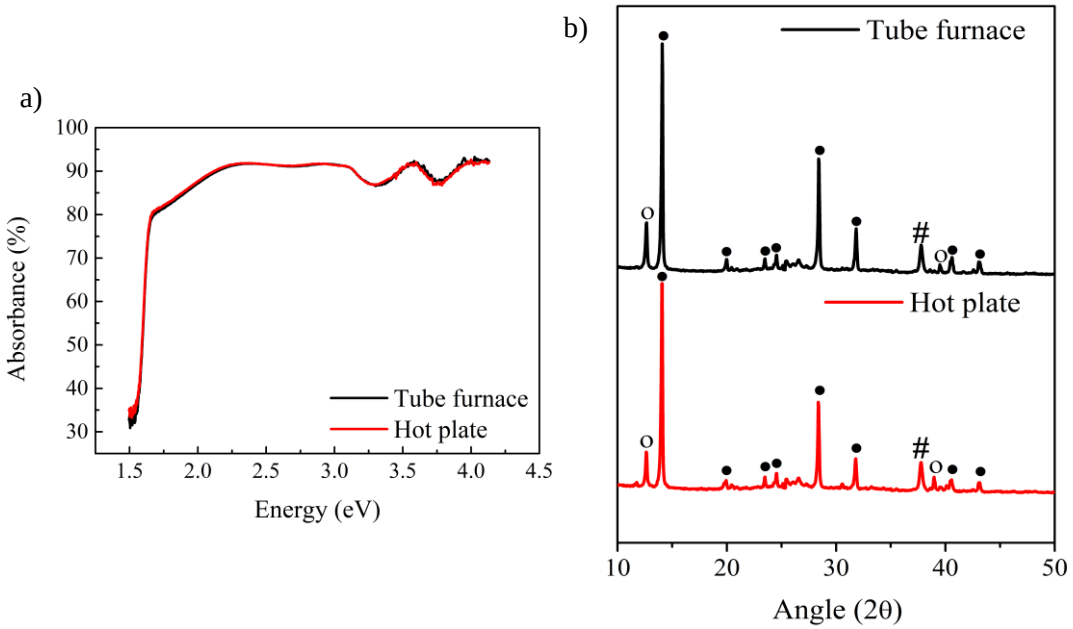

Figure 10 | a) Absorbance spectra and b) XRD for perovskite deposited over c:TiO_2 using TTIP precursor solution in a hot plate and tube furnace. Perovskite layer was annealed in hotplate was done for 15min at 90ºC and tube furnace was an annealing program at RT to 90 ºC for 40 min and remaining 15 min.

Figure 11 reveals SEM images for these two parameters. SEM images were treated by ImageJ software, through which 30 measurements were made and the grain size determined. Thereby, Perovskite film fabricated with the annealing on tube furnace and hot plate exhibit a grain size of 287 ± 94 nm and 294 ± 92 nm, respectively. For these cases, there are only small differences registered. Afterwards, an electrical characterization is carried to confirm which method is the most indicated to achieve the expected efficiency results.

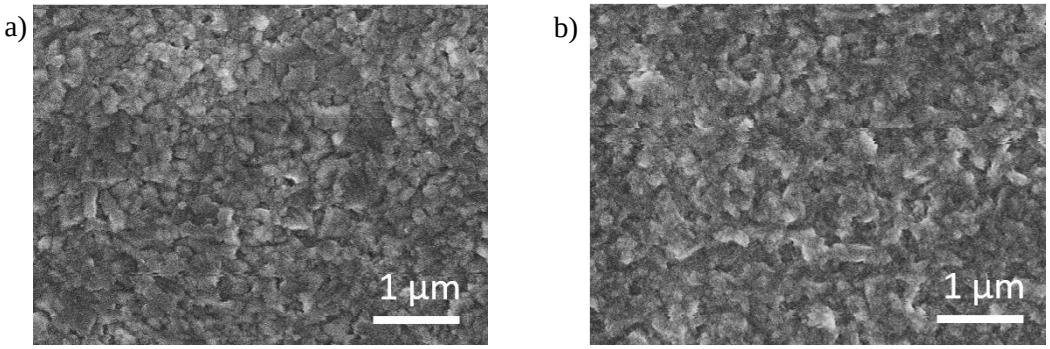

Figure 11 | SEM images for perovskite deposited over c:TiO_2 using TTIP precursor solution in a) a hot plate and b) tube furnace. Perovskite layer was annealed in hotplate was done for 15min at 90ºC and tube furnace was an annealing program at RT to 90ºC for 40 min and remaining 15 min. No CuSCN was deposited.

The *J-V* and *P-V* measurements for the first batch of SC devices are presented in Figure 12, with the details of each measurement being presented in Table 1. All the parameters were extracted from the *I-V* curves of the cells and used the equations from section A of Appendices, to obtain the fill factor (FF), shunt resistance (R_{SH}), series resistance (R_S) and power conversion efficiency (PCE). The differences between them are clear: PSC in which perovskite was annealed in a tube furnace presents an efficiency four times higher compared with the one annealed in a hot plate. However, even the best result shows a low J_{SC} and FF and a very high R_S. The PSC annealed with the tube furnace exhibit a V_{OC}, J_{SC} and FF of 0.76 V, 9.63 mA/cm^2 and 0.23, with a PCE of 1.67%.

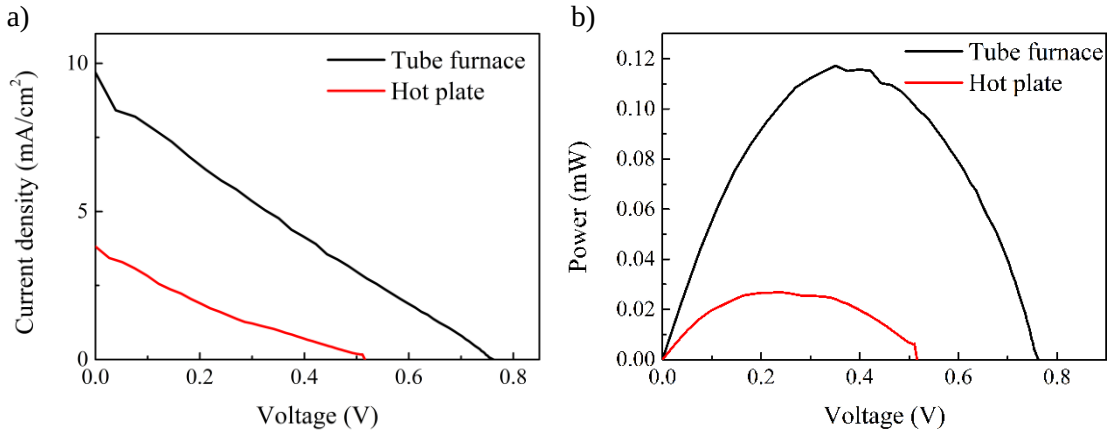

Figure 12 | a) *J-V* and b) *P-V* measurements for solar devices differentiating on anneling methode. Devices fabricated using a compact TiO_2 using TTIP precursor solution; Perovskite layer was annealed in hotplate was done for 15min at 90ºC and tube furnace was a annealing program at RT to 90ºC for 40 min and remain 15 min. 120µL of CuSCN was droped and it is dissolved in di-n-propyl sulfide.

Table 1 | Performance values for the data presented in Figure 12.

	V_{OC} (V)	J_{SC} (mA/cm^2)	FF	R_{SH} (Ω)	R_S (Ω)	PCE (%)
Tube furnace	0.76	9.63	0.23	972	1 251	1.67
Hot plate	0.52	3.89	0.20	1 394	2 933	0.38

3.2.2 Using two differents TiO_2 precursor solution

The correlation between TiO_2 and the crystallographic quality of the perovskite film [49],[50] reveals how important is the TiO_2 layer to the perovskite morphology, as it is stated within the scientific community. In this part of the study, it was investigated the use of two different TiO_2 precursors for development of SCs.

Absorbance spectra shows a high absorption for booth TiO_2 precursors, values between 87-91% and a band gap of approximately 1.52 eV (it is expected since is the same as the last section). XRD characterization enables us to observe the peaks corresponding to the tetragonal phase of $MAPbI_3$ marked with a full circle [45],[46],[47], the PbI_2 peak marked with an empty circle [48], and also peaks regarding the FTO layer marked with a cardinal [45], both shown in Figure 38 from section D of Appendices. These results demonstrate that optically and structurally, no difference may be noted. However, when the cells are electrically characterized, it becomes possible to see some differences.

Figure 13 shows the *J-V* and *P-V* measurements for SCs produced though two different TiO_2 precursors with the corresponding performance values in Table 2. SC produced with compact TiO_2 layer from TTIP precursor (1) improves all parameters, especially PCE which increased more than double. The extremely low J_{SC} and FF confirms the presence of a very high R_S, probably induced by the presence of precursor products for both c:TiO_2 solutions [49]. Additionally, other reason for a high series resistance may be the large thickness of the TiO_2 layer [47]. It needs to be considered the fact that TiO_2 using Acetylacetone solution has a lower speed in spin-coating than TiO_2 using TTIP and it is known that thickness decreases with the increase in speed.

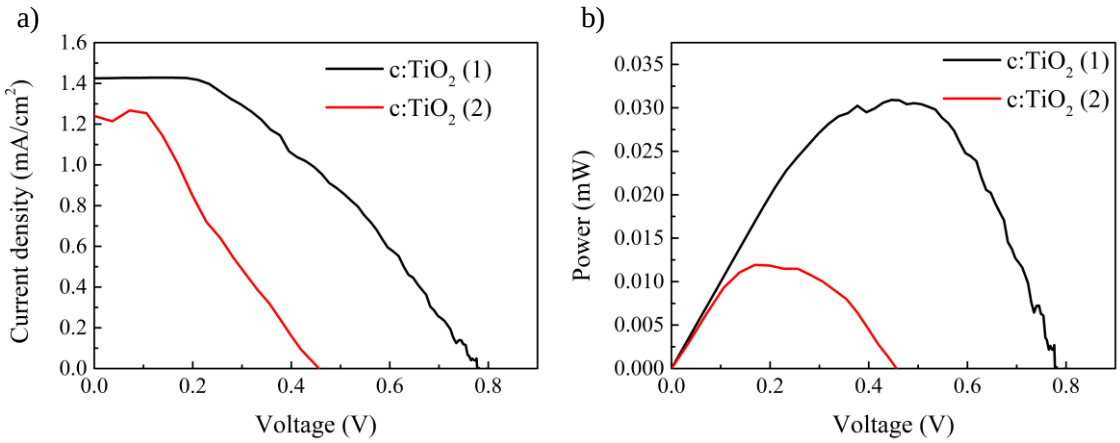

Figure 13 | a) *J-V* and b) *P-V* measurements for solar devices differentiating on compact ETL: c:TiO_2 using TTIP precursor solution (TiO_2 (1)) and using Acetylacetone (TiO_2 (2)). Perovskite layer was described in section Experimental. 120µL of CuSCN was dropeded and it is dissolved in di-n-propyl sulfide.

Table 2 | Performance values for the data presented in Figure 13.

	V_{OC} (V)	J_{SC} (mA/cm^2)	FF	R_{SH} (Ω)	R_S (Ω)	PCE (%)
c:TiO_2 (1)	0.79	1.42	0.39	50 630	3 847	0.44
c:TiO_2 (2)	0.45	1.24	0.30	10 600	4 744	0.17

3.2.3 Effect of different architectures in filtered/unfiltered perovskite solutions

Until this session only the planar architecture for the PSCs was used. From here the influence of the different structures will be studied: planar and compact as well as the factor of doping the mesoporous layer with Li^+.

Theoretically, the addition of mp:TiO_2 layer enhances the performance of the PSCs once it improves light absorption and V_{OC} comparing to the compact architecture [36] [35]. With lithium doping, an increase in SC efficiency is also expected, due to better charge collection [37].

Fabricated devices were done in a planar structure it was investigated the influence of the mesoporous TiO_2 layer with and without Li^+ doping to improve the device.

Figure 14 illustrates the difference in brightness, colour and smoothness in the samples that were used unfiltered and filtered perovskite solutions. In the sample where the filtered solution was used it was observed a shining, dark and smooth surface, although there were some imperfections on this surface that were made during the spin-coating. Nevertheless, when the filtration is not performed, the film obtained is not homogenous.

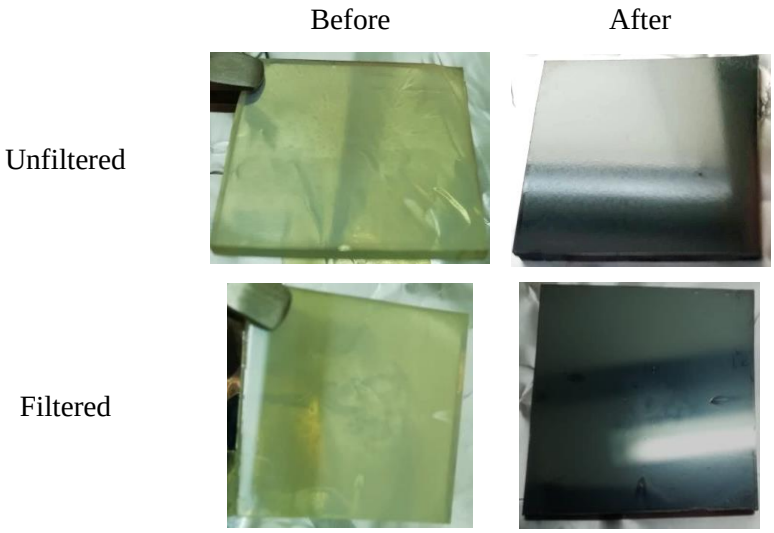

Figure 14 | Images of the samples using the unfiltered and filtered solution of perovskite. The Perovskite was deposited over mesoscopic architecture with Li+ doping. The Perovskite layer was annealed as described in section Experimental. 120µL of CuSCN was dropped and it is dissolved in di-n-propyl sulfide.

a. Unfiltered perovskite solution

From the optical spectra (Figure 15 a)), there is a decrease in the absorption of light with the addition of the mesoporous layer and with the Li^+ doping. This is expected since the mesoporous layer is opaque, which makes it more difficult for the light to go through. Band gap values were obtained with values of 1.48, 1.5 and 1.52 eV to planar, mesoscopic architecture and Li^+ doped mesoscopic architecture, respectively. Consequently, it is possible to report that band gap increases with the addition of these layers. Figure 15 b) reveals the XRD spectra of SCs produced on planar, mesoscopic and Li^+ doped mesoscopic architecture. The XRD results demonstrate the presence of the tetragonal perovskite crystal structure, marked with full circle [45],[46],[47], the PbI_2 peak marked with an empty circle [48], and also peaks regarding the TiO_2 and FTO layer marked with an asterisk and a cardinal, respectively [5], [45] . Predictably, the peaks of TiO_2 in anatase phase rose due to the increased thickness of ETL layer. These samples exhibit a considerably high PbI_2 peak, indicating a high degree of organic degradation.

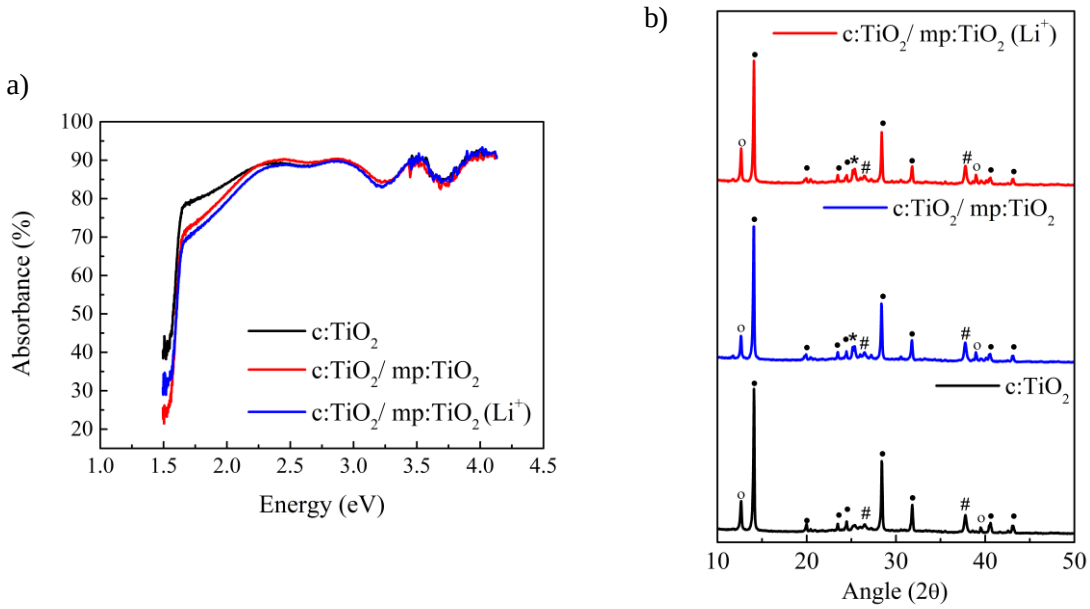

Figure 15 | a) Absorbance and b) XRD spectra for perovskite deposited over c:TiO_2 using TTIP precursor (black), mp:TiO_2 (blue) and Li^+ doping (red). The unfiltered perovskite solution was deposited as described in section Experimental. For this measurements, CuSCN was not deposited.

The SEM images (Figure 16 a), b) and c)) prove the morphology of perovskite film for these SC structures. The grain reaches a size of 260.2 ± 81.5 nm, 312.5 ± 75.8 nm and 350.6 ± 75.4 nm for c:TiO_2, mp:TiO_2 and mp:TiO_2 doped with Li^+, respectively. Hence, it was possible to confirm that the size of the grain increases with the addition of these layers. In short, this is what we are looking for since the larger grain size the better will be the performance of the solar cell [23].

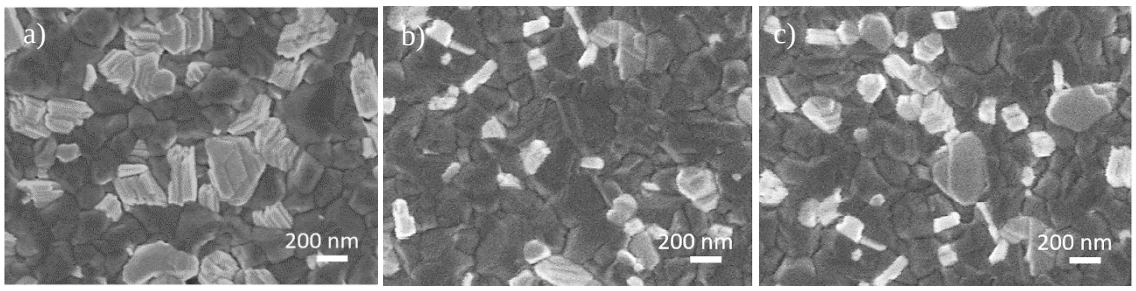

Figure 16 | SEM images for perovskite deposited over a) c:TiO_2 using TTIP precursor, b) mp:TiO_2 and c) Li^+ doping. The unfiltered perovskite solution was deposited as described in section Experimental. For this measurements, CuSCN was not deposited.

Moreover, SEM-EDS of the perovskite's image in mesoscopic architecture doped with Li^+ (Figure 39 from section D of Appendices) was done to confirm the presence of the SC elements. This ensures that the surface is not homogeneous, as verified in Figure 39 d) and e). The zone marked with a) exhibits more intense titanium peak, which may be indicative of the mp:TiO_2 layer on the surface. On a similar note, when comparing region b) with c) it is possible to verify a more intense Sn peak due to the thick FTO layer, which indicates a non-homogeneous perovskite surface.

The electrical measurements for SCs produced on planar, mesoscopic architecture and Li^+ doped mesoscopic architecture in an unfiltered perovskite solution are presented in Figure 17 with the corresponding performance values in Table 3. The performance of PSC based on the mp:TiO_2 illustrates the best efficiency in this section, yielding a value of 1.13%. The J_{SC}, V_{OC} and FF values obtained from curves were 6.40 mA/cm^2, 0.56V and 0.33, respectively. Meanwhile, lithium doping slightly improved FF when compared to planar architecture, despite the low efficiency of 0.15%.

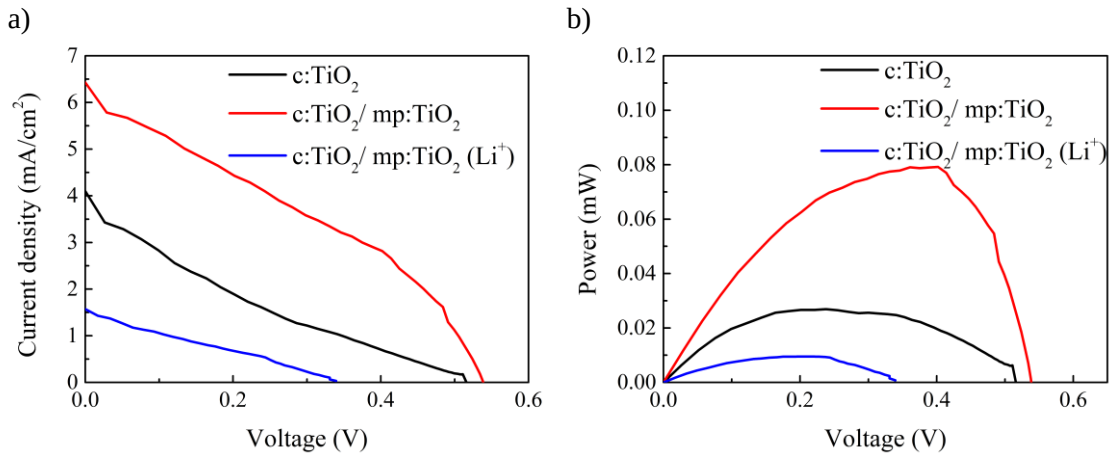

Figure 17 | a) *J-V* and b) *P-V* measurements for solar devices with the addition of c:TiO_2 (black), mp:TiO_2 undoped (red) and doped with Li^+ (red). The unfiltered perovskite solution was deposited as described in section Experimental. 120µL of CuSCN was dropped and it is dissolved in di-n-propyl sulfide.

Table 3 | Performance values for the data presented in Figure 17.

	V_{OC} (V)	J_{SC} (mA/cm²)	FF	R_{SH} (Ω)	R_S (Ω)	PCE (%)
c:TiO_2	0.51	4.10	0.17	1 194	2 833	0.37
c:TiO_2/mp:TiO_2	0.56	6.40	0.33	1 432	605	1.13
c:TiO_2/mp:TiO_2(Li^+)	0.34	1.53	0.25	1 449	2 941	0.15

b. Filtered perovskite solution

The production of a uniform and homogenous film is crucial to get a device with a great execution. Consequently, filtering the perovskite solution may be the key to achieve high performance devices, since this method is practiced by the scientific community [44], [47], [51].

An absorbance between 90-94% is shown in Figure 40 from section D of Appendices, which is highlighted. The perovskite films fabricated on the planar, mesoscopic architecture with and without Li^+ doping presents a band gap of 1.55, 1.52 and 1.5 eV, respectively. For this reason, a decrease of the band gap with the addition of these layers is verified, contrary to what was confirmed in the unfiltered perovskite solution.

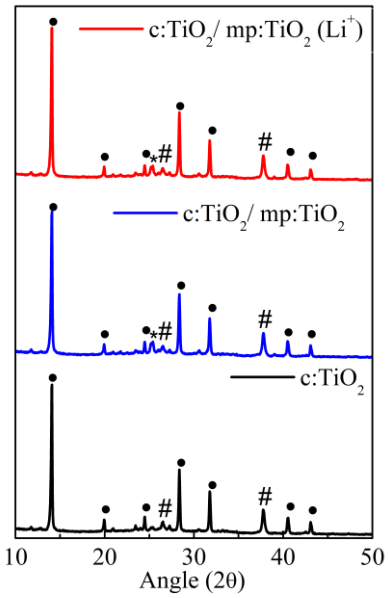

Figure 18 | XRD spectra for filtered perovskite solution deposited over c:TiO_2 using TTIP precursor (black), mp:TiO_2 (blue) and Li^+ doping (red). The perovskite solution was deposited as described in section Experimental. For this measurements, CuSCN was not deposited.

The XRD results (Figure 18) exhibited the presence of the tetragonal perovskite crystal structure, marked with full circle [45],[46],[47], as well as peaks regarding the TiO_2 and FTO layer marked with an asterisk and a cardinal, respectively [5], [45]. The relative intensities of the (110) and (220) planes at an angle 2θ of 14.1º and 28.5º, respectively, increased with the addition of Li^+ doping indicating the improved crystallinity of perovskites and an increased orientation of crystalline domains [52]. In contradiction to the previous section, once the solution has been

filtered, it is not possible to verify PbI_2 peaks.

The perovskite film was examined by SEM (Figure 19 a), b) and c)), it shows that with the planar architecture the grain size is 259.47 ± 56.81 nm, with the addition of mesoporous layer there is an increase (307.64 ± 62.80 nm), and the one with the doping of Li^+ obtains 332.93 ± 94.46 nm of grain size. Thus, the grain size increases with the addition of these layers such as standard deviation, i.e. when perovskite is deposited on top of c:TiO_2, the grain size is more uniform. The presence of elements of each layer (FTO/ TiO_2/ $MAPbI_3$) can be confirmed by SEM-EDS through Figure 41 from section D of Appendices.

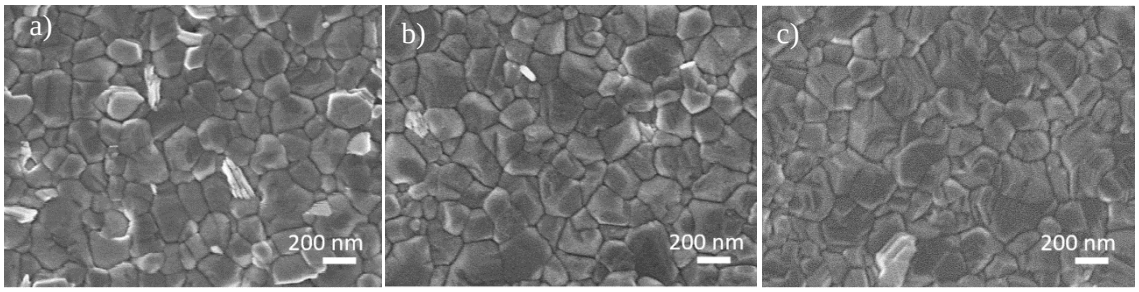

Figure 19 | SEM images for filtered perovskite solution deposited over a) c: TiO_2 using TTIP precursor, b) using a mp: TiO_2 and c) Li^+ doping. The Perovskite layer was annealed as described in section Experimental. For this measurements, CuSCN was not deposited.

Figure 20 shows the *J-V* and *P-V* measurements from the best contact of SCs produced in planar, mesoscopic architecture and Li^+ doping and using filtered perovskite solution with the corresponding performance values in Table 4. Li^+ doped solar cell's parameters show an overall improvement. It is important to highlight the remarkable increase of efficiency corresponding to 8 times higher than the device with the compact layer. The best cell of this batch (i.e., Li^+ doped mesoporous layer) exhibit t a V_{OC} of 0.71 V, J_{SC} of 8.69 mA/cm^2, FF of 36%, and PCE of 2.22%. Therefore, with this increase of performance, it was proved that the Li^+ doping enables faster electron transport within the mesoporous TiO_2 electrodes [37] . It was also demonstrated that PSCs prepared on such electrodes achieved substantially higher performances compared with undoped electrodes improving PCEs from 1.86 to 2.22%. Moreover, a significant enhancement of almost 50% was achieved for the fill factor (FF), which was improved from 22% to 36%.

Table 4 | Performance values for the data presented in Figure 20.

	V_{OC} (V)	J_{SC} (mA/cm^2)	FF	R_{SH} (Ω)	R_S (Ω)	PCE (%)
c:TiO_2	0.54	2.38	0.22	1 687	3 411	0.28
c:TiO_2/m:TiO_2	0.69	9.86	0.27	1 197	859	1.86
c:TiO_2/m:TiO_2(Li^+)	0.71	8.69	0.36	1 109	498	2.22

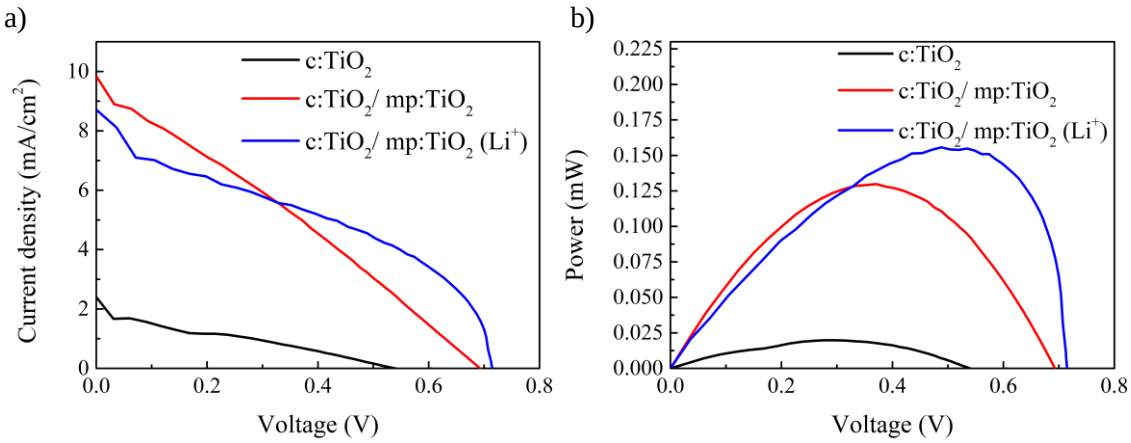

Figure 20 | a) *J-V* and b) *P-V* measurements for solar devices with the addition of c:TiO_2 (black), mp: TiO_2 undoped (red) and doped with Li^+ (blue). The Perovskite was deposited as described in section Experimental . 120µL of CuSCN was dropped and it is dissolved in di-n-propyl sulfide.

3.2.4 Effect of perovskite loading time

As previously stated, the mesoporous layer increases the surface-area of ETL/perovskite [35],[36], thus the time that perovskite needs to be soak in the mesoporous matrix (defined as loading time) will be investigated below. Three loading times for perovskite deposition were studied:10, 30 and 40 s.

The absorbance spectra behavior shown in Figure 42 a) from section D of Appendices demonstrates that there is no difference in band gap between perovskite samples having different loading time. Those perovskite layers deposited on the mesoscopic architecture present a band gap of approximately 1.54 eV and absorbance values are between 90-93% . Images of each cell having loading time 10, 30 and 40 s revels a dark-brown colour and high brightness. They are exhibited in Figure 45 from section F of Appendices.

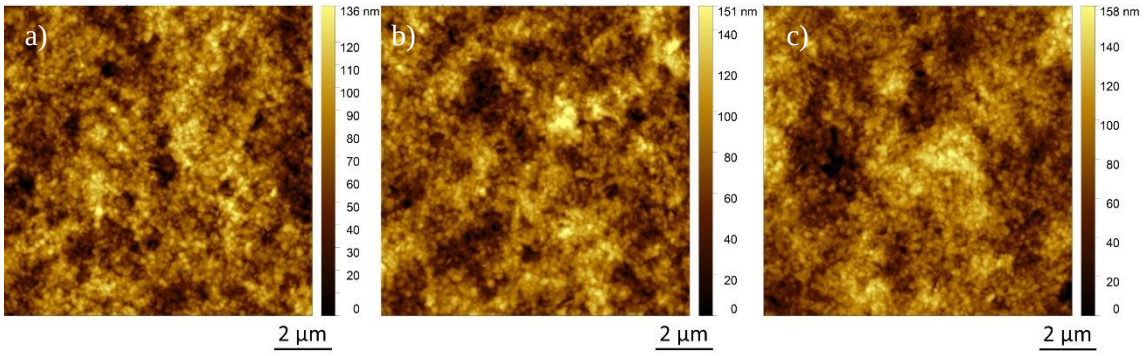

Figure 21 | a), b) and c) AFM images for filtered perovskite solution for different perovskite load time: 10 , 30 and 40 s , respectively. The Perovskite layer was deposited as described in Experiemental. For this measurements, CuSCN was not deposited.

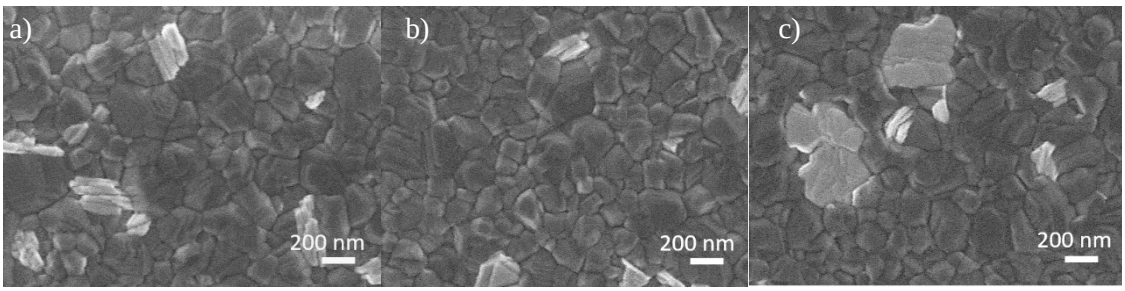

Figure 22 | a), b) and c) SEM images for filtered perovskite solution for different perovskite load time: 10 , 30 and 40 s , respectively. The Perovskite layer was deposited as described in Experiemental. For this measurements, CuSCN was not deposited.

The XRD shown in Figure 42 b) from section D of Appendices confirmed the presence of the tetragonal perovskite crystal structure marked with full circle [45],[46],[47] and peaks regarding the TiO_2 and FTO layer marked with an asterisk and a cardinal, respectively [5], [45]. This characterization also reveals peaks of PbI_2 (marked with an empty circle [48]), indicating perovskite's degradation. However, the structural results between these three times are similar. AFM images (Figure 21) were treated using Gwyddion software and only one measure was performed. A uniform film is present with roughness of 22.64, 25.24 and 26.36 nm for 10, 30 and 40 s of loading time, correspondingly (Table 5). Therefore, the roughness increases with the perovskite's loading time due to the solution being dipped into the scaffold TiO_2 during this period. Figure 22 revels the SEM image for different load time tested in this work. The grain size obtained for 10, 30 and 40 s of loading time is 324.9 ± 86.9, 331.4 ± 75.9 and 312.3 ± 65.9 nm, respectively (Table 5). A large grain size is favourable since it is associated to large grain boundaries and low recombination.

Table 5 | Influence of different loading time on $MAPbI_3$ roughness and grain domain size.

Loading time	10 s	20 s	30 s
Roughness (nm)	22.64	25.24	26.36
Grain Size (nm)	260.2 ± 81.5	312.5 ± 75.8	350.6 ± 75.4

The electrical characterization is presented in Figure 23 with the details of each measurement being detailed in Table 6. It was achieved 2.86% of PCE, 0.46 of FF and 8.69 mA/cm^2 of J_{SC} for the cell with 30 s of perovskite's loading time, becoming the best performance for this parameter. Both performances for 10 and 40 s are lower than expected, however it has a great V_{OC} (approximately 0.9 V). In short, the ideal period that perovskite should be loaded is 30 s. Thereby, it can be penetrated the mesoporous layer long enough to fill the bulks.

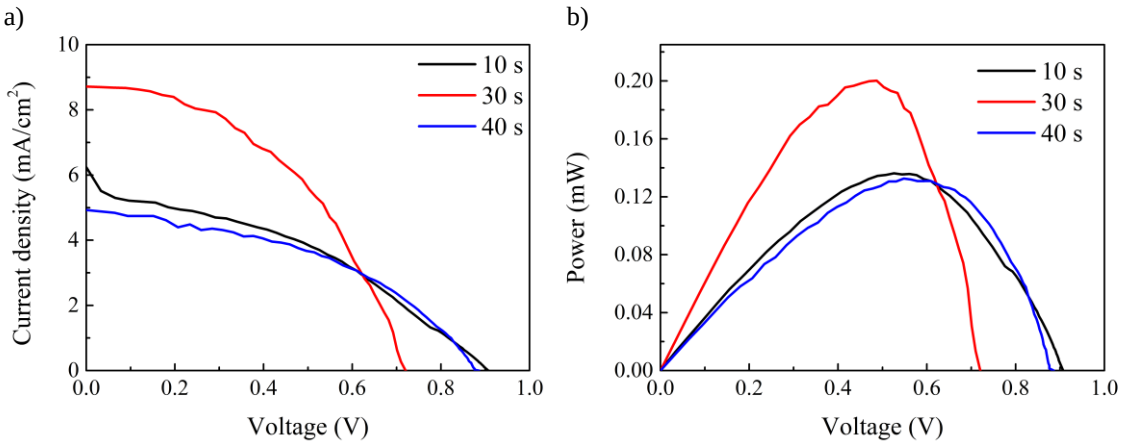

Figure 23 | a) *J-V* and b) *P-V* measurements for solar devices with load time variation: 10 s (black), 30 s (red) and 40 s (blue). The Perovskite layer was deposited as described in section Experimental. 120µL of CuSCN was dropped and it is dissolved in di-n-propyl sulfide.

Table 6 | Performance values for the data presented in Figure 23.

Loading time	V_{OC} (V)	J_{SC} (mA/cm^2)	FF	R_{SH} (Ω)	R_S (Ω)	PCE (%)
10 s	0.90	6.25	0,34	2 366	1 236	1.95
30 s	0.72	8.69	0,46	5 490	582	2.86
40 s	0.87	4.93	0,43	6 080	995	1.89

3.2.5 Effect of chrolobenzene

As referred in the introduction, the chlorobenzene deposition is a step used to increase nucleation's velocity although it leads to defects in the film as spatially inhomogeneous nucleation [29]. Therefore, to obtain a better performance of PSC, the volume of anti-solvent (120 µL and 100 µL) along with the influence of making it a chlorobenzene's atmosphere in spin-coater was tested. The last procedure consisted of creating a chlorobenzene's atmosphere by dripping a small amount of the solvent (100 µL) inside the spin coater. According to literature, it guarantees an increase of reproducibility [53].

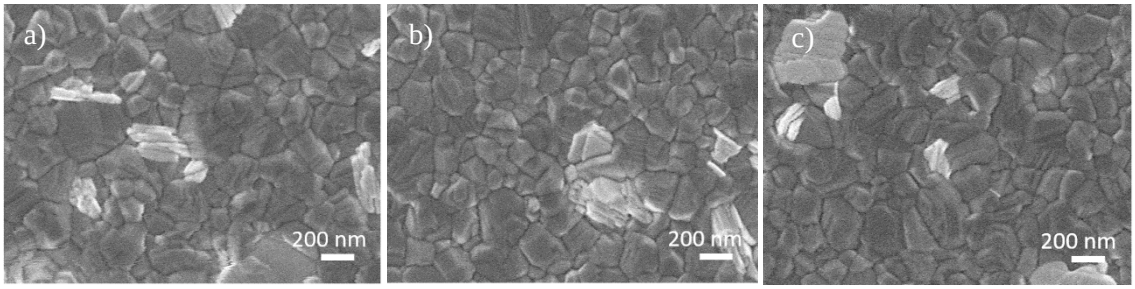

Figure 24 | SEM images for filtered perovskite solution deposited over mesoporous layer for different amonts of chlorobenzene: a) 100 µL, b) 120 µL and with chlorobenzene inside spin-coater c). The Perovskite layer was deposited with the parameters described in section Experimental. For this measurements, CuSCN was not deposited.

These three parameters present a similar band gap and absorbance (Figure 43 from section D of Appendices). Those perovskite layer deposited on a mesoscopic architecture reveal a band gap of approximately 1.54 eV and the absorbance values are between 86-92%. SEM images (Figure 24) show that grain size increases with the amount of anti-solvent. With 100µL and 120 µL of chlorobenzene the grain size is 266 ± 73 nm and 275 ± 58 nm, respectively. For the case where chlorobenzene is placed inside the spin-coating it is possible to observe a grain size of 259 ± 86 nm.

The Perovskites SCs electrical characterization are shown in Figure 25 and the parameters calculated from it are present in Table 7. Perovskite prepared with 120 µL of chlorobenzene exhibited lower results compared with the other two cases. When it fabricated with 100 µL of chlorobenzene, it allows a PSC efficiency of 4.14 mA/cm^2 with a V_{OC} of 0.74 V, J_{SC} of 14.27 mA/cm^2, FF of 0.39. On the other hand, when an atmosphere of chlorobenzene in spin-coater is made, it is obtained V_{OC} of 0.81 V, J_{SC} of 15.34 mA/cm^2, FF of 0.35 and PCE of 4.42%. In conclusion, when only 100 µL of chlorobenzene is used without an atmosphere of chlorobenzene, the results achieved are favourable.

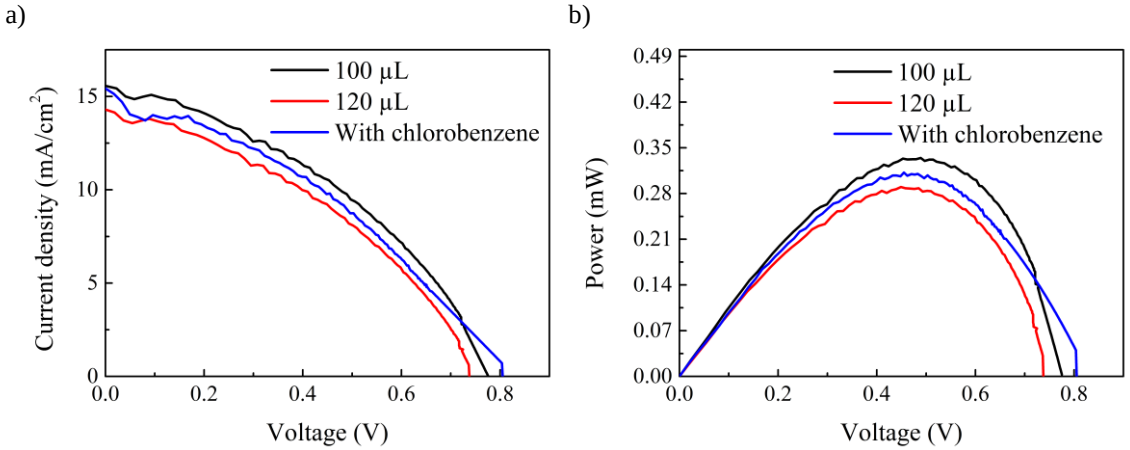

Figure 25 | a) *J-V* and b) *P-V* measurements for solar devices. The filtered perovskite solution was deposited over mesoporous layer with different amonts of chlorobenzene: 100 µL (black), 120 µL (red) and with chlorobenzene inside spin-coater (blue). 120µL of CuSCN was dropped and it is dissolved in di-n-propyl sulfide.

Table 7 | Performance values for the data presented in Figure 25.

Chlorobenzene	V_{OC} (V)	J_{SC} (mA/cm^2)	FF	R_{SH} (Ω)	R_S (Ω)	PCE (%)
100 µL	0.78	15.57	0.36	1 547	339	4.78
120 µL	0.74	14.27	0.39	1 692	345	4.14
With	0.81	15.34	0.35	1 366	470	4.42

3.2.6 Filtered CuSCN dissolved in di-n-propyl sulfide

It is known that HTL layer helps protect the perovskite layer from degradation. Therefore, the way that CuSCN's deposition is done strongly influences the results achieved [38]. Considering that the CuSCN could not be well dissolved and in order to obtain a good interaction between these two layers, it was tested the effect of filtering the CuSCN solution dissolved in di-

n-propyl sulfide. Figure 46 from section E of Appendices shows some perovskite solar cells from this batch where it is possible to observe the difference of brightness for the case of filtered (a) and b)) and unfiltered CuSCN (c) and d)). As performed for the other parameters, optical and structural characterization were done, shown in Figure 26. An absorbance's average of 92% and a band gap of 1.53 and 1.54 eV for the deposition of the filtered and unfiltered CuSCN layer, respectively, are achieved. XRD characterization exhibits the presence of the tetragonal perovskite crystal structure (full circle) [45],[46],[47], peaks regarding the TiO_2 and FTO (asterisk and cardinal, respectively) [5], [45] and also peaks corresponding to CuSCN (cross) [54]. Clearly, the perovskite film with the filtered solution leads to more intense peaks which is indicative of a more crystalline film.

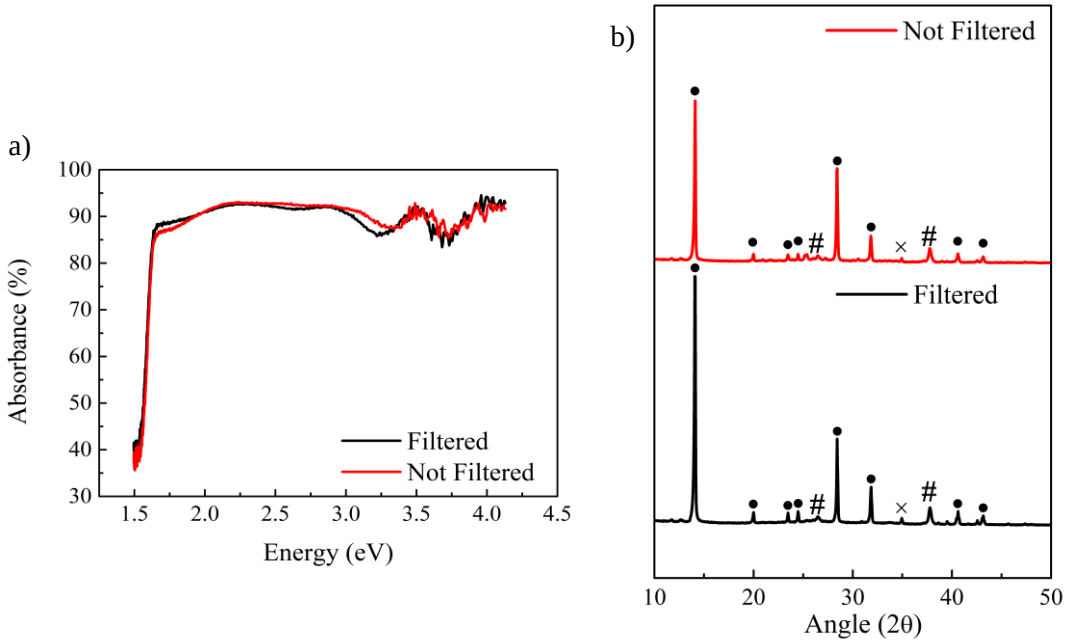

Figure 26 | a) Absorbance spectra and b) XRD for solar devices with filtered and not filtered CuSCN dissolved in di-n-propyl sulfide solution. The Perovskite layer was annealed as described in section Experimental. 120µL of CuSCN was dropped.

These devices were electrically characterized, and the *J-V* and *P-V* curves are illustrated in Figure 27. The extracted V_{OC}, J_{SC}, FF, R_{SH}, R_S and PCE are summarized in Table 8. By comparison, obvious difference can be seen between filtered and unfiltered CuSCN dissolved in di-n-propyl sulfide. The J_{SC}, V_{OC} and FF values obtained from the curves of the filtered CuSCN solution were 15.46 mA/cm^2, 0.89V and 0.46, respectively, yielding a PCE of 6.35%. These were the best results during this optimization study. In contrast, the corresponding J_{SC}, V_{OC} and FF values from electrical measurements of the unfiltered solution were 11.1mAcm^{-2}, 0.78V and 0.36, respectively. In conclusion, this process allowed an almost doubled efficiency improvement compared to the unfiltered CuSCN solution.

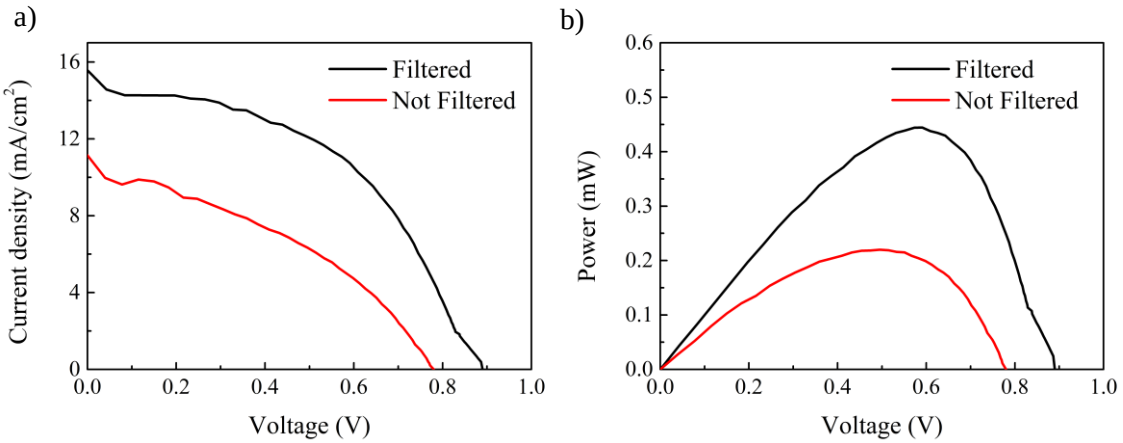

Figure 27 | a) *J-V* and b) *P-V* measurements with filtered and not filtered CuSCN dissolved in di-n-propyl sulfide solution. The Perovskite layer was annealed as described in section Experimental. 120µL of CuSCN was dropped.

Table 8 | Performance values for the data presented in Figure **27**27.

CuSCN	V_{OC} (V)	J_{SC} (mA/cm^2)	FF	R_{SH} (Ω)	R_S (Ω)	PCE (%)
Filtered	0.89	15.46	0.46	2 516	356	6.35
Not filtered	0.78	11.10	0.36	1 947	489	3.14

SEM-FIB image was taken only two months after manufacturing the PSC due to problems with the equipment. Although the sample was still black, bright and without signs of degradation, it was possible to verify the state of degradation through the SEM images (Figure 28).

The bulk density should be as high as possible, however, due to the conditions of the SC at that time, it was not possible to provide any comments about it. The thickness of each layer was calculated trough ImageJ. The cross section of the SC showed a thickness of 297.4 nm for the FTO layer, of 47.5 nm for the compact TiO_2, of 623.9 nm for mesoporous and perovskite and 36 nm of CuSCN. There is no differentiation between mesoporous and perovksite layers due to the perovskite being sucked into the TiO_2 matrix. EDS characterization was done in order to confirms the presence of the elements of each layer (Figure 29).

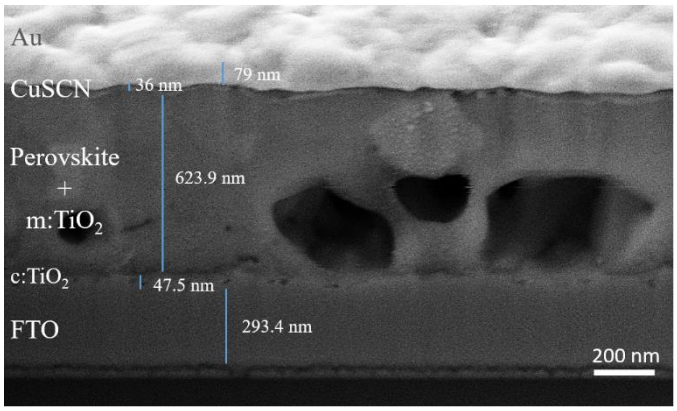

Figure 28 | SEM-FIB: cross section of a $MAPbI_3$ solar cell produced with filtered CuSCN solution.

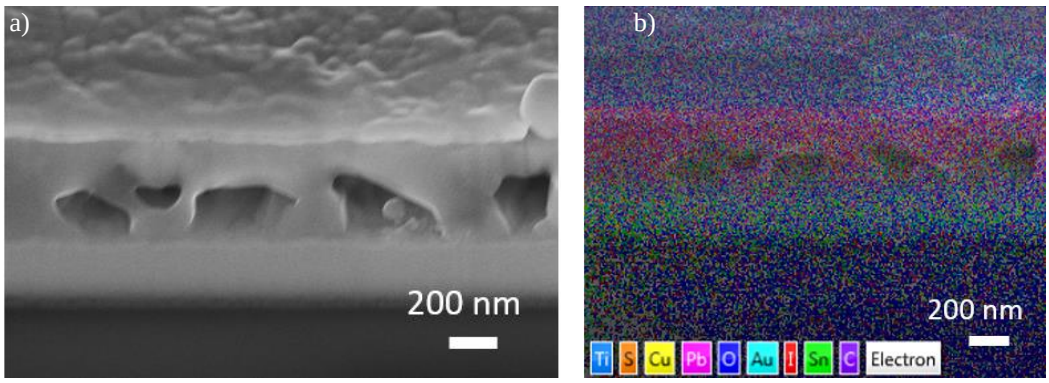

Figure 29 | a) SEM and b) EDS mapping of the cross section of a MAPbI3 solar cell produced with filtered CuSCN solution.

3.2.7 Different solutions of CuSCN

So far, only CuSCN dissolved in di-n-propyl sulfide was used for device optimization due to delivering time of the reagents. In this study two different solution for HTL were used: CuSCN dissolved in di-n-propyl sulfide (1) and CuSCN dissolved in diethyl sulfide (2), both unfiltered.

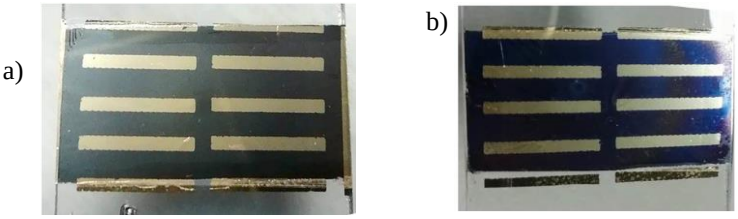

Figure 30 | Images of the samples with a) CuSCN dissolved in di-n-propyl sulfide and b) dissolved in diethyl sulfide.

A few differences of brightness and colour on the top of the solar cell are revealed in Figure 30 and also in Figure 47 from section E of Appendices. The SC with CuSCN (1) present a darker colour compared with the blue colour of CuSCN (2) Absorbance spectra behaviour is exhibited in Figure 31 a) and no differences between these two solutions are noted. Those exhibit an absorbance between 87-92% and a band gap of, approximately, 1.53 eV.

XRD characterization, in Figure 31 b), displays the presence of the tetragonal perovskite crystal structure marked with full circle [45],[46],[47], peaks regarding the TiO_2 and FTO layer marked with an asterisk and a cardinal, respectively [5], [45] and also peaks corresponding to CuSCN marked with a cross [54]. This demonstrates that the perovskite film produced below CuSCN (2) exhibits higher intensity peaks, i.e., it is more crystalline.

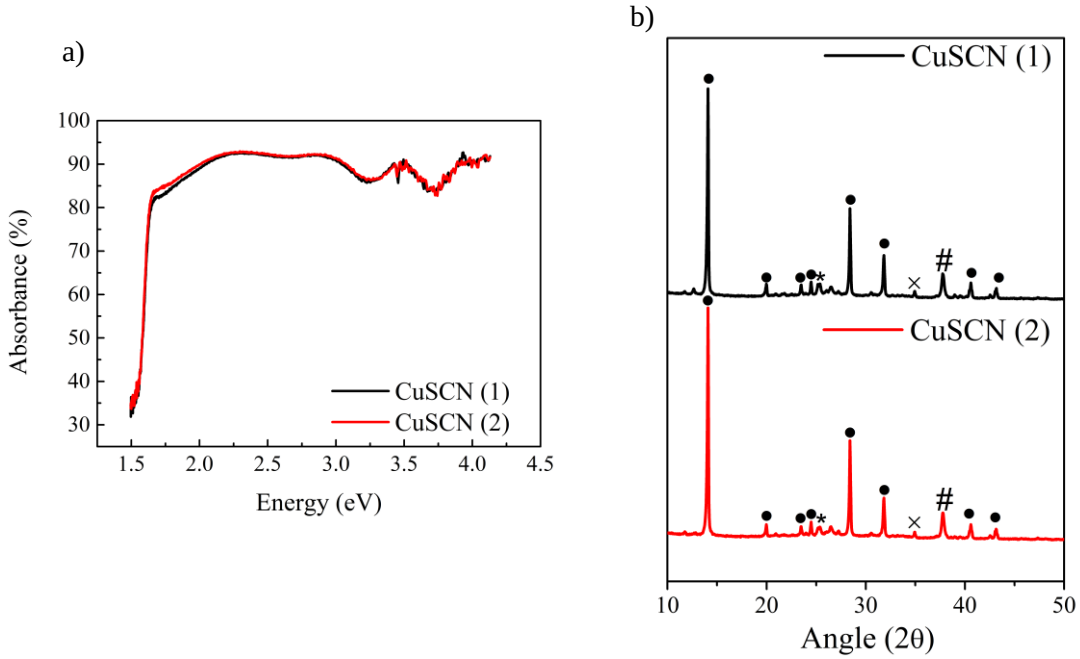

Figure 31 | a) Absorbance spectra and b) XRD for solar devices with diferent solutions of CuSCN (dissolved in di-n-propyl sulfide solution- CuSCN (1) and dissolved in diethyl sulphide- CuSCN (2)). The Perovskite layer was annealed as described in section Experimental. 120µL of CuSCN (1) and CuSCN (2) unfiltered solution was dropped, respectively.

As in the previously section, electrical characterization was made, which is illustrated in Figure 32 with the corresponding performance values in Table 9. PSC fabricated with CuSCN (2) exhibit a value of J_{SC}, V_{OC}, R_S and R_{SH} of 10.62 mA/cm^2, 0.62 V, 1632 Ω and 392 Ω, respectively, yielding a PCE of 2.38%, in opposition with 12.67 mA/cm2, 0.53 V, 1566 Ω and 424 Ω, allowing a PCE of 3.51% for the CuSCN (1). This value is 1.5 times higher than the one for solar cells fabricated with CuSCN dissolved in diethyl-sulphide.

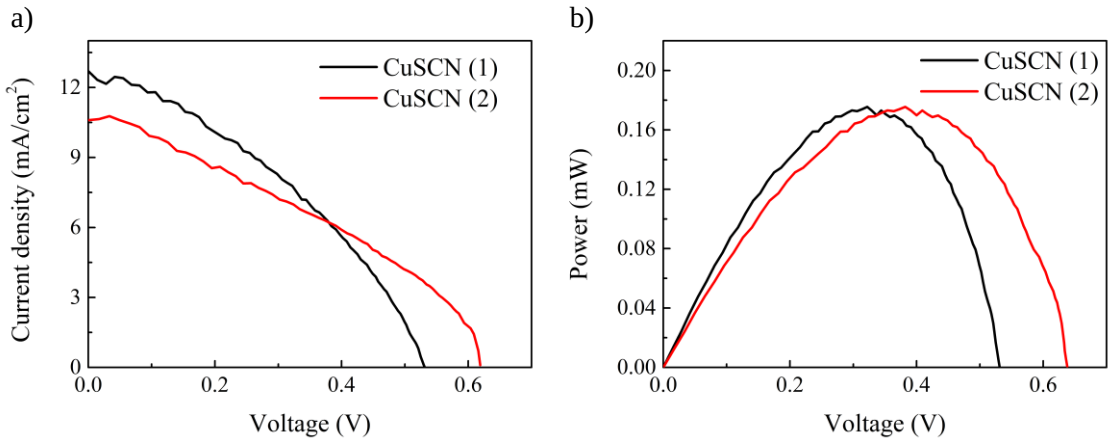

Figure 32 | a) *J-V* and b) *P-V* measurements with diferent solutions of CuSCN (dissolved in di-n-propyl sulfide solution- CuSCN (1) and dissolved in diethyl sulphide- CuSCN (2)). The Perovskite layer was annealed as described in section Experiemntal. 120µL and 35 µL of CuSCN (1) and CuSCN (2) unfiltered solution was dropped, respectively.

Table 9 | Performance values for the data presented in Figure 32.

	V_{OC} (V)	J_{SC} (mA/cm^2)	FF	R_{SH} (Ω)	R_S (Ω)	PCE (%)
CUSCN (1)	0.53	12.67	0.37	1 566	424	3.51
CUSCN (2)	0.62	10.62	0.36	1 632	392	2.38

It was expected that PCE would be closer to the obtained in section 3.2.6 of Results and Discussion, since this PSC made with CuSCN (1) have the same procedure. The only uncontrolled parameter was the moisture, which presented a humidity level of 62% in this batch and in the last (section 3.2.6) was of 56%.

Consequently, other studies have also been carried out to optimize PCS. The influence of the solution's volume to be dropped for HTL was analysed. However, this study had results lower than expected since the moisture was quite high, above 66%.

Volumes of 35 µL and 120 µL of CuSCN solutions, both unfiltered, were studied. Thus, electrical measurements were done and they are shown in Figure 44 from section E of Appendices with the respective performance values in Table 10. PSC fabricated with 35 µL CuSCN dissolved in di-n-propyl sulfide presents the best performance with a V_{OC}, J_{SC} and PCE of 0.84 V, 7.49 mA/cm^2 and 1.76%.

Table 10 | Performance values for the data presented in Figure 44 from section E of Appendices.

CuSCN	V_{OC} (V)	J_{SC} (mA/cm^2)	FF	R_{SH} (Ω)	R_S (Ω)	PCE (%)
(1) 35 µL	0.84	7.49	0.28	1 486	1 432	1.76
(1) 120 µL	0.71	2.11	0.20	3 490	6 969	0.30
(2) 35 µL	0.67	2.72	0.23	2 340	3 707	0.42
(2) 120 µL	0.65	0.82	0.23	7 660	10 840	0.12

3.3 Perovskite's degradation

A brief study was performed on SC to investigate the effect of moisture and time on the device's performance as well as in perovskite's degradation.

a. Effect of moisture

As referred above, moisture plays a key role in the solar cell´s parameters. These SCs are manufactured with the same conditions but present very different performances. This is mainly due to the only parameter that was not controlled inside the laboratory: the humidity level. The relative humidity (RH) values were recorded through the dehumidifier.

Figure 33 shows the effect of moisture not only with the SC performance but also with the amount of SCs working. With a very high humidity value is noted that the devices perform poorly. However, when values of humidity are less than 57% is noticeable an increase of PCE as well of

the number of SCs working. It is possible to conclude that solar cells should be produced in environments with a level of humidity less than 57% and it is expected to be more degraded for moisture values above this value.

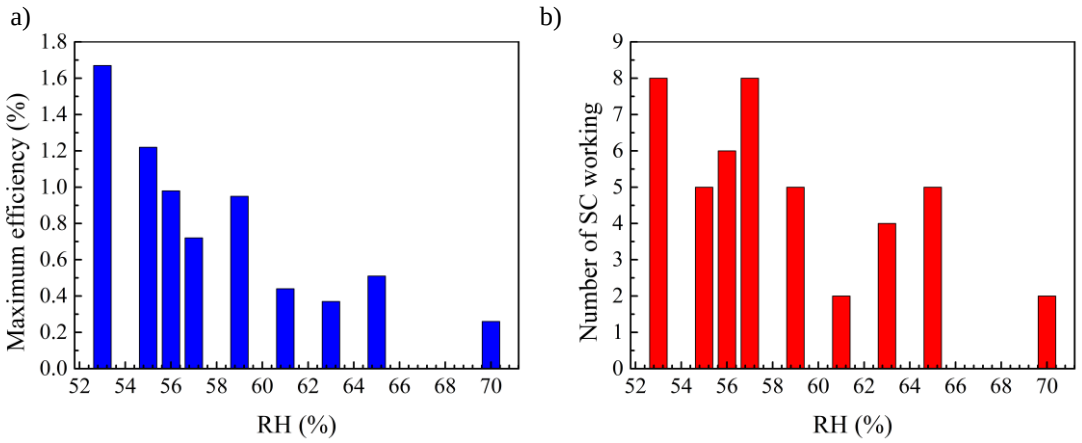

Figure 33 | a) Maximum efficiency in function of relative humidity and b)PCE dependence on the humidity. The recorded moisture values were performed with a batch of 8 cells.

In cases where the number of cells working is eight (8), i.e., the whole batch working, should be taken into account not only the humidity factor but owing to the reproducibility of the process.

b. Effect of time

In this section, PSCs were manufactured with filtered and unfiltered perovskite's solution in a mesoscopic architecture, doped with Li^+ with 30 s of loading time. The CuSCN deposited in this device, it is the one dissolved in di-n-propyl sulfide. Figure 34 shows the impact of the time in PSCs. This SCs were kept in an open Petri dish without controlled atmospheric conditions. The degradation of perovskite is notable at approximately 30 days although the yellow colour is not present. This also translates to better operational stability at non- controlled atmospheric conditions. In addition, it is an optimistic point since in literature is possible to observe a quickly degradation of perovskite films in just 1 day [20][21].

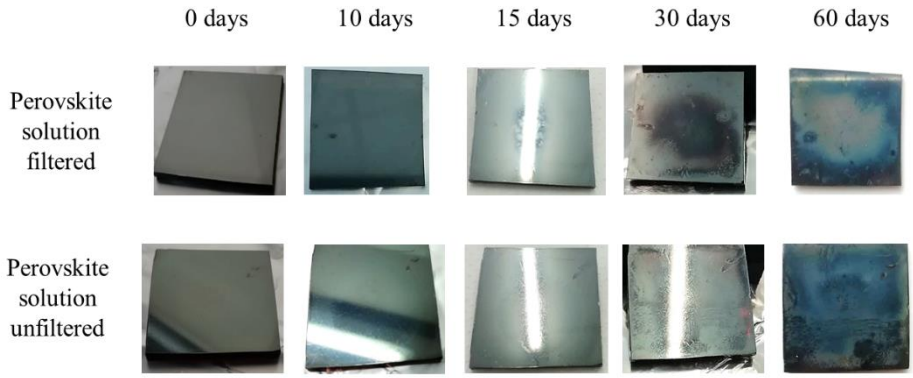

Figure 34 | Degradation observations of encapsulated planar $CH_3NH_3PbI_3$ perovskite solar cells at "uncontrolled"ambient conditions.

4 Conclusions and Future Perspectives

As previously mentioned, one of the main goals of this work was to improve the performance of perovskite solar cells using TiO_2 as Electron Transport Layer (ETL), $CH_3NH_3PbI_3$ as active layer and CuSCN as Hole Transport Layer (HTL). The aim is to also fabricate SCs using low cost, simple and fast production methods. Therefore, optical, structural, morphological and electrical characterizations were performed.

In the first part of this work, two solutions for ETL and HTL were tested. For the ETL, transmittance values between 79-85% are obtained and with the addition of mesoporous layer the transmittance decrease, since this layer has an opaque appearance. In addition, the doped mesoporous layer with Li^+ presents a maximum transmittance close to 90 % and low parasite absorbance (close to 10%) which is a good result since the perovskite will be illuminated through glass FTO-ETL. About HTL, the two films produced with CuSCN dissolved in di-n-propyl sulfide and dissolved in diethyl sulfide present similar results. Moreover, a transmittance average of 85 % and absorbance values between 5-10% are exhibited. This is crucial to avoid overlap with the parasitical absorption of $MAPbI_3$.

On the second part, seven fabrication parameters were changed in order to improve the device: changing the annealing method, using two different solutions for c:TiO_2, altering the SC architecture, influencing of perovskite filtration as well as the anti-solvent volume and using two different solutions for CuSCN layer. XRD and electrical characterization proved that perovskite films annealed in a tube furnace improved the crystallinity of the film and the performance of the device. It was observed that, in general, the band gap of perovskite produced during this work was close to 1.53 eV with an absorbance value of, approximately, 92%. For better morphological proprieties, i.e. to obtain a large grain size, the perovskite may be deposited on a mesoporous architecture doped with Li^+ and the perovskite solution may be filtered and loaded for 30 s so the perovskite can dip into the mesoporous TiO_2 scaffold. Moreover, XRD verified the presence of a perovskite film in the tetragonal phase with (110), (112),(211), (202),(220), (310), (224) ,(314) planes at a 2θ angle of 14,1º, 20º, 23.52º, 24.5º, 28.5º, 31.87º, 40.55º, 43.17º respectively. On other hand, when the perovskite's solution was unfiltered, the presence of the PbI_2 phase was observed at 12.67° and 38.7º. This could be caused by device's degradation during their exposure to air or because the solution was not well dissolved. Unlike filtered solution where PbI_2 phase was not exhibit. Also, in this matter, the CuSCN dissolved in diethyl sulfide is recommended since it increases the crystallinity of perovskite's film.

The J_{SC} and V_{OC} values obtained from the *J-V* and *P-V* curves of the best solar cell produced were 15.46 mA/cm^2 and 0.89V, respectively, yielding a PCE of 6.35% under standard AM 1.5 conditions. For R_S and R_{SH} values exhibited are 356 and 2516 Ω, respectively, which is a good scope in this work, since ideally, these two parameters present the values: $R_S \approx 0$ and $R_{SH} \approx \infty$. With

this result it is possible to prove that better perovskite films can be easily prepared in our lab even with a relatively high humidity level, suggesting excellent moisture stability. In general, device optimization can be considered a success, as the top reported PCE in the previous work was 2.65% [43], which has now been increased to 6.35%, more than two times the previous efficiency. The best fabrication parameters, within the ones tested, are presented in Table 11.

Table 11 | Final fabrication conditions for PSCs

Annealing	Tube furnace
ETL	TiO_2 (TTIP solution) with a mesoporous layer doped with Li^+
Perovskite layer	Filtered solution with a loading time of 30 s
Volume of anti-solvent	100 µL without a chlorobenzene's atmosphere
HTL	Filtered solution of CuSCN dissolved in di-n-propyl sulfide

Regarding perovskite degradation, more precisely, the influence of moisture on the perovskite layer and performance, it was observed that the filtered perovskite film begins to show signs of degradation after 30 days, while the unfiltered does not appear to have such degradation. In short, solar cells should be manufactured in environments with a humidity level lower than 57%.

4.1.1 Future perspectives

When using the standard architecture, a study should be carried out to understand if there is an improvement in the SC operation when transparent Titania paste is used [55], since the light can go through this layer (ETL) even better and further illuminate the active layer.

It should be carried out a more detailed study about CuSCN since this layer has a very important role in the device. Studies such as filtering effect in both solutions performed in this work: CuSCN dissolved in di-n-propyl sulfide and dissolved in diethyl sulfide. Furthermore, the velocity during the spin should also be investigated.

Finally, an investigation about the use of IZO between the CuSCN layer and the gold should be taken into account, since researchers have already reported an improvement in efficiency with the use of this material [56]. Another material to be also used as a spacer layer with much interest is the graphene oxide due to being cheaper and being able to stabilize the perovskite layer [38].

As a more general future perspective, it would be interesting to further investigate the effect of moisture on film morphology as well as the degradation of the perovskite during constant illumination with temperature and to discover ways of it being avoided. It would also be appealing to study alternative materials for each layer in the PSC structure to try to optimize the cell and see if other materials reduce degradation as well as the applicability in reversed and flexible SCs.

References

[1] A. Polman, M. Knight, E. C. Garnett, B. Ehrler, and W. C. Sinke, "Photovoltaic materials: Present efficiencies and future challenges," *Science (80-.).*, vol. 352, no. 6283, p. aad4424–aad4424, 2016.

[2] J. M. Ball, M. M. Lee, A. Hey, and H. J. Snaith, "Low-temperature processed meso-superstructured to thin-film perovskite solar cells," *Energy Environ. Sci.*, vol. 6, pp. 1739–1743, 2013.

[3] G. A. Casas, M. A. Cappelletti, A. P. Cédola, B. M. Soucase, and E. L. Peltzer y Blancá, "Analysis of the power conversion efficiency of perovskite solar cells with different materials as Hole-Transport Layer by numerical simulations," *Superlattices Microstruct.*, vol. 107, pp. 136–143, 2017.

[4] H. S. Jung and N. G. Park, "Perovskite solar cells: From materials to devices," *Small*, vol. 11, no. 1, pp. 10–25, 2015.

[5] L. Qiu *et al.*, "Fabrication of high efficiency perovskite solar cells based on mesoporous TiO2 nanofibrous film under high humidity conditions," *Mater. Res. Bull.*, vol. 106, no. June, pp. 439–445, 2018.

[6] O. Almora, L. Vaillant-Roca, and G. Garcia-Belmonte, "Perovskite Solar Cells: A brief Introduction and some Remarks," *Rev. Cuba. Física*, vol. 34, no. 1, pp. 58–68, 2017.

[7] P. Vivo, J. K. Salunke, and A. Priimagi, "Hole-Transporting Materials for Printable Perovskite Solar Cells," *Materials (Basel).*, vol. 10, no. 1087, pp. 1–45, Sep. 2017.

[8] A. H. Reshak, M. M. Shahimin, and I. F. Fauzi, "Drift and Diffusion Component Studies in CdTe Structure for Photovoltaic Application," *Int. J. Electrochem. Sci.*, vol. 9, no. 2, pp. 700–709, 2014.

[9] M. I. H. Ansari, A. Qurashi, and M. K. Nazeeruddin, "Frontiers, opportunities, and challenges in perovskite solar cells: A critical review," *J. Photochem. Photobiol. C Photochem. Rev.*, vol. 35, pp. 1–24, 2018.

[10] H. Atwater and A. Polman, "Plasmonics for improved photovoltaic devices," *Nat. Mater.*, vol. 9, pp. 205–214, 2010.

[11] S. Prasanthkumar and L. Giribabu, "Recent Advances in Prevoskite-Based Solar Cells," *Curr. Sci.*, vol. 111, no. 7, pp. 1173–1181, 2016.

[12] M. Saliba *et al.*, "Cesium-containing triple cation perovskite solar cells: improved stability, reproducibility and high efficiency," *Energy Environ. Sci.*, vol. 9, pp. 1989–1997, 2016.

[13] K. Amnuyswat and P. Thanomngam, "Effect of exchange-correlation and GW approximations on electrical property of cubic, tetragonal and orthorhombic CH3NH3PbI3," *Integr. Ferroelectr.*, vol. 177, pp. 1–9, 2017.

[14] M. A. Green, A. Ho-Baillie, and H. J. Snaith, "The emergence of perovskite solar cells," *Nat. Photonics*, vol. 8, no. July, pp. 506–514, 2014.

[15] P. Gao, M. Gratzel, and M. K. Nazeeruddin, "Organohalide Lead Perovskites for Photovoltaic Applications," *Energy Environ. Sci.*, vol. 7, pp. 2448–2463, 2014.

[16] M. Ye, X. Hong, F. Zhang, and X. Liu, "Recent advancements in perovskite solar cells: flexibility, stability and large scale," *J. Mater. Chem. A*, vol. 4, no. 18, pp. 6755–6771, 2016.

[17] M. Valles-Pelarda *et al.*, "Analysis of the Hysteresis Behavior of Perovskite Solar Cells with Interfacial Fullerene Self-Assembled Monolayers," *J. Phys. Chem. Lett.*, vol. 7, no. 22, pp. 4622–4628, 2016.

[18] I. K. Popoola, M. A. Gondal, and T. F. Qahtan, "Recent progress in flexible perovskite solar cells: Materials, mechanical tolerance and stability," *Renew. Sustain. Energy Rev.*, vol. 82, pp. 1–25, 2017.

[19] J. Troughton, K. Hooper, and T. M. Watson, "Humidity resistant fabrication of $CH_3NH_3PbI_3$ perovskite solar cells and modules," *Nano Energy*, vol. 39, pp. 60–68, 2017.

[20] S. N. Habisreutinger, D. P. McMeekin, H. J. Snaith, and R. J. Nicholas, "Research Update: Strategies for improving the stability of perovskite solar cells," *APL Mater.*, vol. 4, 2016.

[21] A. Al Mamun, Y. Mohammed, T. T. Ava, G. Namkoong, and A. A. Elmustafa, "Influence of air degradation on morphology, crystal size and mechanical hardness of perovskite film," *Mater. Lett.*, 2018.

[22] Q. Chen *et al.*, "Under the spotlight: The organic-inorganic hybrid halide perovskite for optoelectronic applications," *Nano Today*, vol. 10, no. 3, pp. 355–396, 2015.

[23] Y. Luo, F. Meng, E. Zhao, Y. Z. Zheng, Y. Zhou, and X. Tao, "Fine control of perovskite-layered morphology and composition via sequential deposition crystallization process towards improved perovskite solar cells," *J. Power Sources*, vol. 311, pp. 130–136, 2016.

[24] X. Tong, F. Lin, J. Wu, and Z. M. Wang, "High performance perovskite solar cells," *Adv. Sci.*, vol. 3, no. 5, pp. 1–18, 2015.

[25] W. Nie *et al.*, "High-efficiency solution-processed perovskite solar cells with millimeter-scale grains," *Science (80-.).*, vol. 347, no. 6221, pp. 522–525, 2015.

[26] N. J. Jeon, J. H. Noh, Y. C. Kim, W. S. Yang, S. Ryu, and S. Il Seok, "Solvent engineering for high-performance inorganic-organic hybrid perovskite solar cells," *Nat. Mater.*, vol. 13, no. 9, pp. 897–903, 2014.

[27] Y. Gao *et al.*, "Anti-solvent surface engineering via diethyl ether to enhance the photovoltaic conversion efficiency of perovskite solar cells to 18.76%," *Superlattices Microstruct.*, vol. 113, pp. 761–768, 2018.

[28] H. Bazzazzadegan, Y. Mortazavi, A. Khodadadi, and M. Mohagheghian, "Large-grain $CH_3NH_3PbI_3$ film by incorporation of urea in one-step solution process," *Superlattices Microstruct.*, 2018.

[29] N. Yaghoobi Nia, M. Zendehdel, L. Cinà, F. Matteocci, and A. Di Carlo, "A Crystal Engineering Approach for Perovskite Solar Cells and Modules Fabrication out of the Glove Box," *J. Mater. Chem. A*, 2017.

[30] L. Wang, G. R. Li, Q. Zhao, and X. P. Gao, "Non-precious transition metals as counter electrode of perovskite solar cells," *Energy Storage Mater.*, vol. 7, pp. 40–47, 2017.

[31] G. A. Sepalage *et al.*, "A facile deposition method for CuSCN: Exploring the influence of CuSCN on J-V hysteresis in planar perovskite solar cells," *Nano Energy*, vol. 32, pp. 310–319, 2017.

[32] I. Jeong *et al.*, "Solution-Processed Ultrathin TiO_2 Compact Layer Hybridized with Mesoporous TiO_2 for High-Performance Perovskite Solar Cells," *ACS Appl. Mater. Interfaces*, pp. 1–33, 2017.

[33] S. Wang *et al.*, "Enhanced performance of TiO_2-based perovskite solar cells with Ru-doped TiO_2 electron transport layer," *Sol. Energy*, vol. 169, pp. 335–342, 2018.

[34] S. S. Shin *et al.*, "High-performance flexible perovskite solar cells exploiting Zn_2SnO_4 prepared in solution below 100 °C," *Nat. Commun.*, vol. 6, no. 7410, pp. 1–8, 2015.

[35] M. Abdi-jalebi *et al.*, "Impact of a Mesoporous Titania − Perovskite Interface on the Performance of Hybrid Organic − Inorganic Perovskite Solar Cells," *J. Phys. Chem. Lett.*, vol. 7, no. 16, pp. 3264–3269, 2016.

[36] A. Marchioro *et al.*, "Unravelling the mechanism of photoinduced charge transfer processes in lead iodide perovskite solar cells," *Nat. Photonics*, vol. 8, no. 3, pp. 250–255, 2014.

[37] F. Giordano *et al.*, "Enhanced electronic properties in mesoporous TiO_2 via lithium doping for high-efficiency perovskite solar cells," *Nat. Commun.*, vol. 7, p. 10379, 2016.

[38] N. Arora *et al.*, "Perovskite solar cells with CuSCN hole extraction layers yield stabilized efficiencies greater than 20%," *Science (80-.).*, vol. 358, no. 6364, pp. 768–771, 2017.

[39] P. Qin *et al.*, "Inorganic hole conductor-based lead halide perovskite solar cells with 12.4% conversion efficiency," *Nat. Commun.*, vol. 5, pp. 1–6, 2014.

[40] J. M. Ball *et al.*, "Optical properties and limiting photocurrent of thin-film perovskite solar cells," *Energy Environ. Sci.*, vol. 8, no. 2, pp. 602–609, 2015.

[41] J. W. Jung, C. C. Chueh, and A. K. Y. Jen, "High-Performance Semitransparent Perovskite Solar Cells with 10% Power Conversion Efficiency and 25% Average Visible Transmittance Based on Transparent CuSCN as the Hole-Transporting Material," *Adv. Energy Mater.*, vol. 5, no. 17, pp. 1–7, 2015.

[42] A. Fonseca, "Perovskite Solar Cells: Developing a simple, fast and low-cost fabrication technology," *Master thesis, Univ. Nov. Lisboa*, 2017.

[43] E. Duarte, "Low-Cost Thin Film Perovskite Solar Cells," *Master thesis, Univ. Nov. Lisboa*, 2018.

[44] Q. Zhou, Z. Jin, H. Li, and J. Wang, "Enhancing performance and uniformity of $CH_3NH_3PbI_3$-xClx perovskite solar cells by air-heated-oven assisted annealing under various humidities," *Sci. Rep.*, vol. 6, pp. 1–8, 2016.

[45] G. Rajendra Kumar *et al.*, "Phase transition kinetics and surface binding states of methylammonium lead iodide perovskite," *Phys. Chem. Chem. Phys.*, vol. 18, no. 10, pp. 7284–7292, 2016.

[46] A. Mei *et al.*, "A hole-conductor-free, fully printable mesoscopic perovskite solar cell with high stability.," *Science*, vol. 345, no. 6194, pp. 295–298, 2014.

[47] S. S. Mali, C. K. Hong, A. I. Inamdar, H. Im, and S. E. Shim, "Efficient planar n-i-p type heterojunction flexible perovskite solar cells with sputtered TiO_2 electron transporting layers," *Nanoscale*, vol. 9, pp. 3095–3104, 2017.

[48] L.-M. Chao, T.-Y. Tai, Y.-Y. Chen, P.-Y. Lin, and Y.-S. Fu, "Fabrication of $CH_3NH_3PbI_3$/PVP Composite Fibers via Electrospinning and Deposition," *Materials (Basel).*, vol. 8, no. 8, pp. 5467–5478, 2015.

[49] B. Conings *et al.*, "An easy-to-fabricate low-temperature TiO_2 electron collection layer for high efficiency planar heterojunction perovskite solar cells heterojunction perovskite," *APL Mater.*, vol. 2, no. 8, 2015.

[50] P. Vivo *et al.*, "Influence of TiO_2 compact layer precursor on the performance of perovskite solar cells," *Org. Electron. physics, Mater. Appl.*, vol. 41, pp. 287–293, 2017.

[51] Q. Tai *et al.*, "Efficient and stable perovskite solar cells prepared in ambient air irrespective of the humidity," *Nat. Commun.*, vol. 7, pp. 1–8, 2016.

[52] J.-F. Wang *et al.*, "Surface engineering of perovskite films for efficient solar cells," *Sci. Rep.*, vol. 7, no. 1, pp. 1–9, 2017.

[53] T. Schnier, J. Emara, S. Olthof, and K. Meerholz, "Influence of Hybrid Perovskite Fabrication Methods on Film Formation, Electronic Structure, and Solar Cell Performance," *J. Vis. Exp.*, no. 120, pp. 1–8, 2017.

[54] S. Ye *et al.*, "CuSCN-Based Inverted Planar Perovskite Solar Cell with an Average," *Nano*, pp. 3–8, 2015.

[55] T. Duong *et al.*, "Rubidium Multication Perovskite with Optimized Bandgap for Perovskite-Silicon Tandem with over 26% Efficiency," *Adv. Energy Mater.*, vol. 7, no. 14, pp. 1–11, 2017.

[56] H. Shen *et al.*, "Mechanically-stacked perovskite/CIGS tandem solar cells with efficiency of 23.9% and reduced oxygen sensitivity," *Energy Environ. Sci.*, vol. 11, pp. 394–406, 2018.

[57] T. Markvart and L. Castañer, "Practical Handbook of Photovoltaics: Fundamentals and Applications: Fundamentals and Applications," p. 1015, 2003.

[58] Y. Wang *et al.*, "Air-stable, hole-conductor-free high photocurrent perovskite solar cells with $CH_3NH_3PbI_3$–NiO nanoparticles composite," *Nano Energy*, vol. 27, pp. 535–544, 2016.

Appendices

A Solar Cell parameters

In this section the calculations of the solar cell´s parameters are explained through *I-V* and *P-V* curves (Figure 35) where the main equations used for the solar cell´s electrical characterization are presented. Moreover, Figure 36 shows the influence of series resistance (R_S) and shunt resistance (R_{SH}) in the *I-V* curves and in fill factor (FF) [57]. Obviously, for the *J-V* curves shown in this work, they are divided by the current for active area and this should be taken into account for the equations presents bellow.

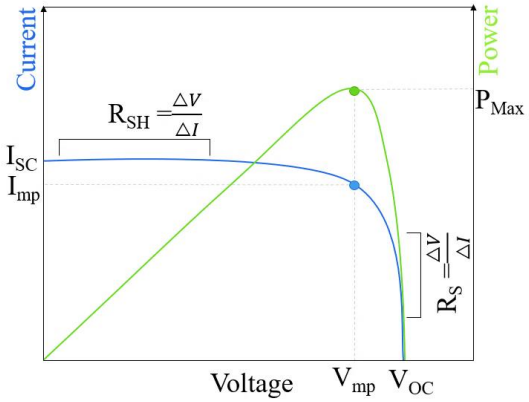

Figure 35 | Illustration of *I-V* and *P-V* curves for calculation of solar cell parameters. Adapted from [57]**.**

In this way:

- Maximum power (P_{Max}) may be calculated:

$$P_{Max} = I_{mp} \times V_{mp} \quad (1)$$

- Fill Factor (FF) is approximate to a square from IV curve and is calculated by:

$$FF = \frac{I_{mp} \times V_{mp}}{I_{SC} \times V_{OC}} \quad (2)$$

- Power conversion efficiency (PCE) is the ratio between maximum P_{Max} and light power (P_{light}) in W/m^2 (1000 W/m^2):

$$PCE = \frac{P_{Max}}{P_{light}} \times 100\% \quad (3)$$

- R_S e R_{SH}, series resistance and shunt resistance, respectively, are obtain by inverse of slope of IV curves. Ideally, these two parameters present the values: $R_S \approx 0$ and $R_{SH} \approx \infty$.

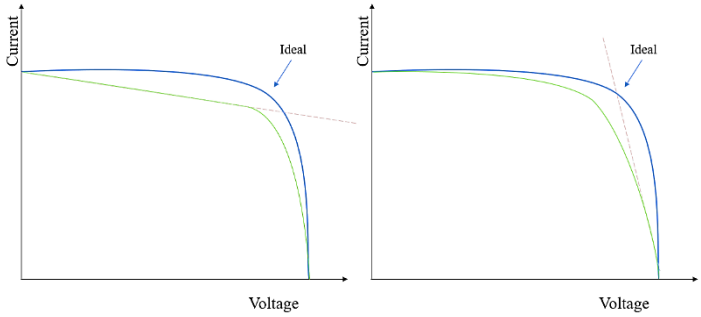

Figure 36 | Influence of series (rigth) and shutt (left) resistance (R_S and R_{SH}) in solar cell performance. Improving series resistence and decreasing shutt resistance may induce the redution of Isc and Voc, respectively. Adapted from [57]**.**

B Materials

This section presents the reagents used during this thesis with respective abbreviation, purity, CAS number and company.

Table 12 | List of reagents used throughout this work with respective abbreviation, purity, CAS and company.

Material	Abbreviation	Purity	Cas Number	Company
Absolute Ethanol	EtOH	99,99%	64-17-5	FISHER CHEMICAL
Acetetonitrile	-	99,5%	75-05-8	SIGMA-ALDRICH
Acetylacetone	-	99,50%	-	FLUKA
Chlorobenzene	-	99%	108-90-7	SIGMA-ALDRICH
Colloidal TiO_2 Paste (22 Nm)	-			SIGMA-ALDRICH
Copper (I) Thiocyanate	CuSCN	96%	1111-67-7	ALFA AESAR
Diethyl Sulfide	-	98%	352-93-2	SIGMA-ALDRICH
Dimethyl Sulfoxide	DMSO	99,90%	67-68-5	FISHER CHEMICAL
Di-N-Propyl Sulfide		98%	111-47-7	ALFA AESAR
Hidrochloric Acid	HCl	37%	7647-01-0	SIGMA-ALDRICH
Lead Iodide	PbI_2	99%	10101-63-0	SIGMA ALDRICH
Lithium Salt	Li-TFSI	99,95%	90076-65-6	SIGMA-ALDRICH
Methylammonium Iodide	MAI	98%	14965-49-2	SIGMA ALDRICH
N-N Dimethylformamide	DMF	99,80%	68-12-2	PANREAC
Titanium (Iv) Isopropoxide	TTIP	97%	546-68-9	SIGMA-ALDRICH
Zinc Powder	-		9029-97-4	JOSÉ M. VAZ PEREIRA

C Solutions preparation

This section presents the recipes for the solutions preparation used in the Experimental section.

1. ETL

The four precursor solutions needed for ETL fabrication were prepared using the following materials: Titanium (IV) Isopropoxide (TTPI), absolute ethanol (EtOH), Hydrochloric acid (HCL) and acetylacetone.

- For the compact TiO_2 (1): The first precursor was prepared by a solution of 18 µL of HCl in 1.286 mL of EtOH, that was dropwise, to a solution of 180 µL of TTIP in 1.286 mL of EtOH and stirred, at least, for 30 min.
- For the compact TiO_2 (2): Other precursor was prepared by a solution of 60 µL of TTIP and 40 µL of Acetylacetone in 0,9 mL EtOH and stirred, at least, for 2 hours.

2. Perovskite precursor solution

The materials used to perform the perovskite precursor solutions were Methylammonium Iodide (MAI), Lead Iodide (PbI_2) powders. As solvent a mix of dimethylformamide (DMF) and dimethyl sulfoxide (DMSO) was used with a ratio (DMF:DMSO) of 4:1.

In other words, the perovskite solution was prepared by dissolving 461 mg PbI_2 and 159 mg MAI in 0,8 ml DMF and 0,2 ml DMSO. These solutions with concentrations of 1M were stirred at 70ºC at least 6h and the substrate was preheated at 70ºC for 10 min on a hotplate.

3. HTL

The precursor solution for HTL fabrication was prepared using a Copper(I) Thiocyanate (CuSCN) powder dissolved in Di-n-propyl sulfide (98%) and in Diethyl sulfide. The concentration of each solution was a concentration of 15 mg/mL and 35 mg/mL, respectively. The first solution was left to stir for 24h at RT and the second solution was stirred 1 hour at RT. The first solution should be preferentially filtered through a syringe filter of 0,2 µm.

D Optical and Structural Characterization

This section presents the optical and structural characterization of ETL layer and of the solar cells structure without the CuSCN layer and Au contacts.

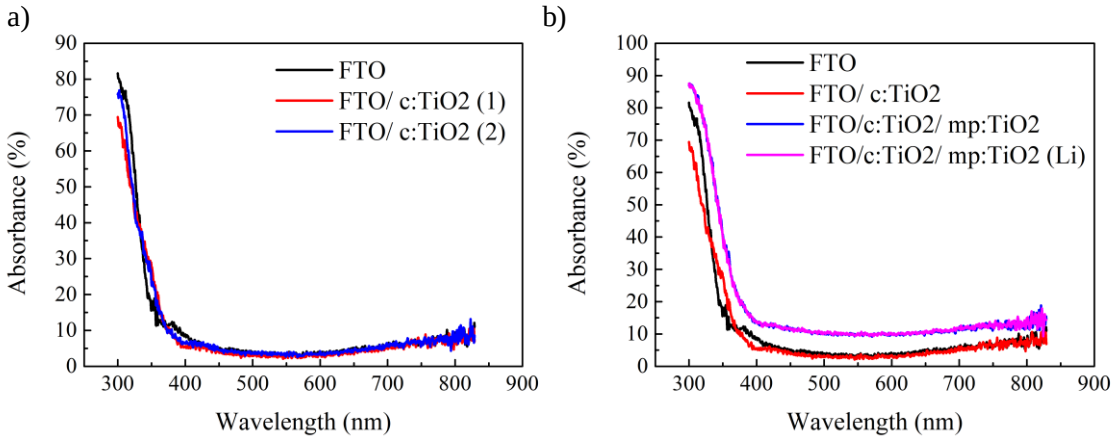

Figure 37 | Absorbance spectra of differents substracts as ETL over FTO (black), a) c:TiO2 (1) and (2) with red and blue, respectively and b) c:TiO2 (red), adding m:TiO2 (blue) and m:TiO2 doped with Li (pink) deposited with the final defined conditions for solar cells fabrication as described in section Experiemtal

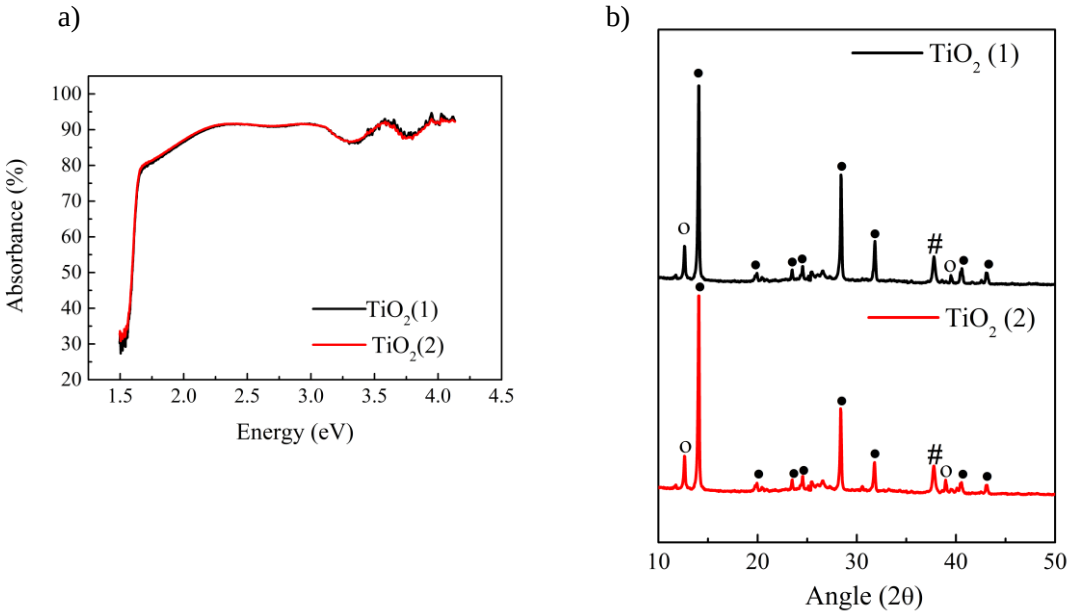

Figure 38 | a) Absorbance spectra and b) XRD for perovskite deposited over different compact ETL: c:TiO_2 using TTIP precursor solution (TiO_2 (1)) and using Acetylacetone (TiO_2 (2)). Perovskite layer was described in section Experimental. For this measurements CuSCN was not deposited.

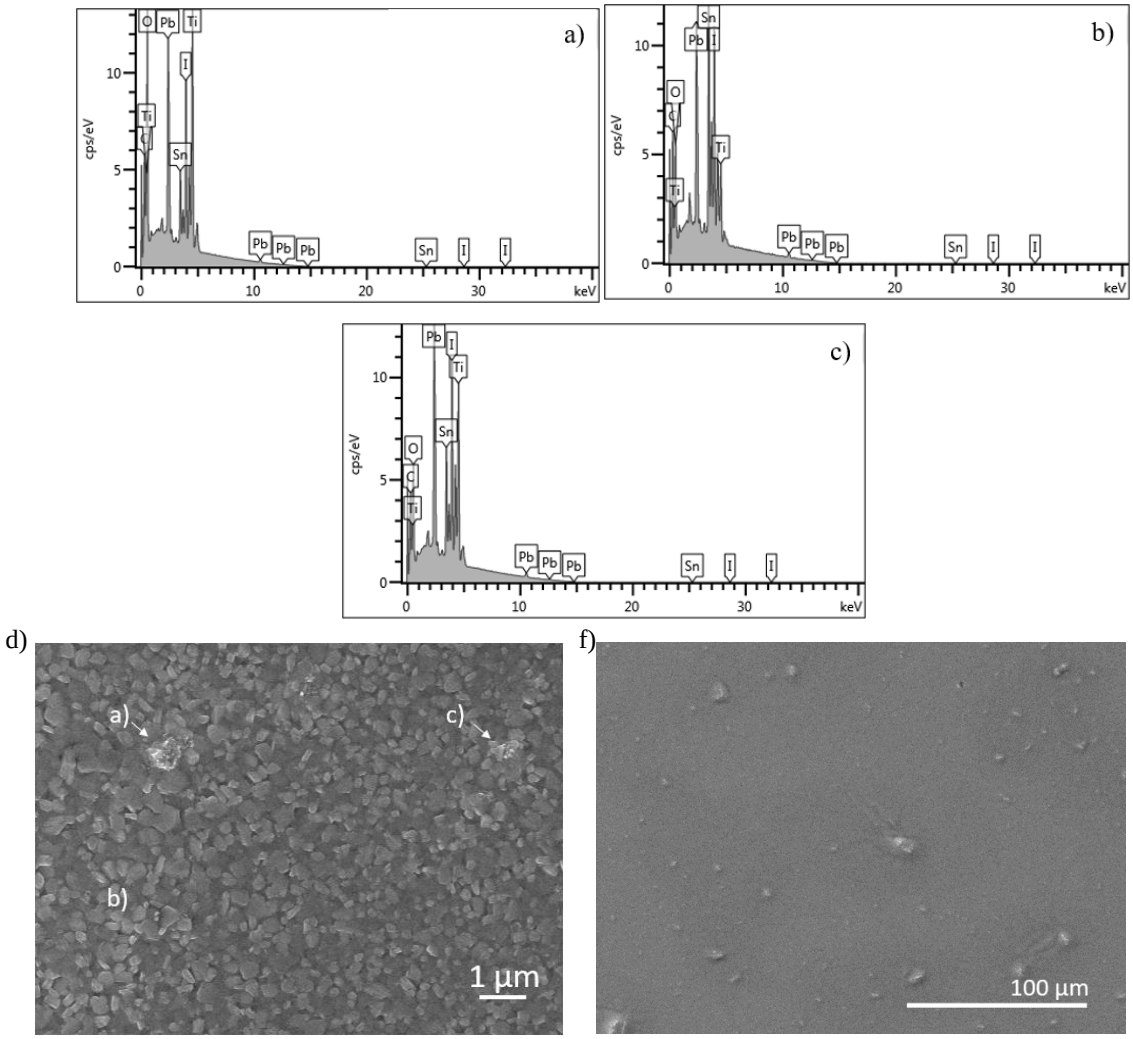

Figure 39 | a), b), c) SEM-EDS characterization, d) and e) SEM image of inhomogeneous perovskite layer. Figure 37 d) and e) are from different areas of perovskite film. The Perovskite layer was deposited as described in Experiemental. For this measurements, CuSCN was not deposited.

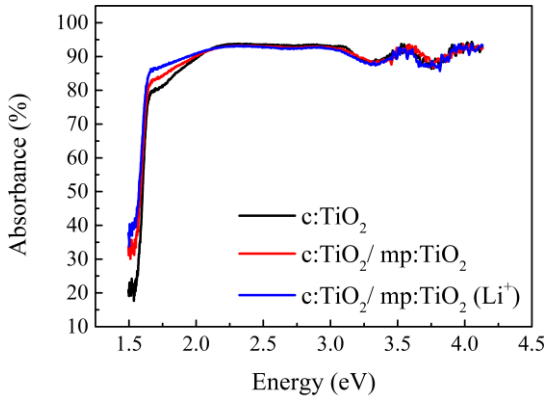

Figure 40 | Absorbance spectra for filtered perovskite solution deposited over c:TiO_2 using TTIP precursor solution (dark points), using a mp: TiO_2 (red points) and Li^+ doping (blue points). The Perovskite layer was deposited as described in section Experimental. 120µL of CuSCN was dropped and it is dissolved in di-n-propyl sulfide.

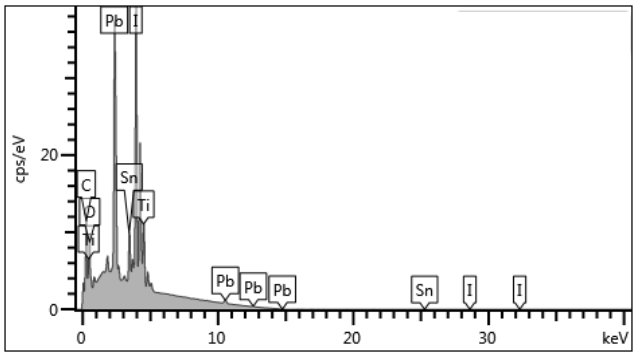

Figure 41 | EDS analysis of perovskite films, deposited over a mesoporours TiO_2. The Perovskite layer was deposited as described in Experiemental. For this measurements, CuSCN was not deposited.

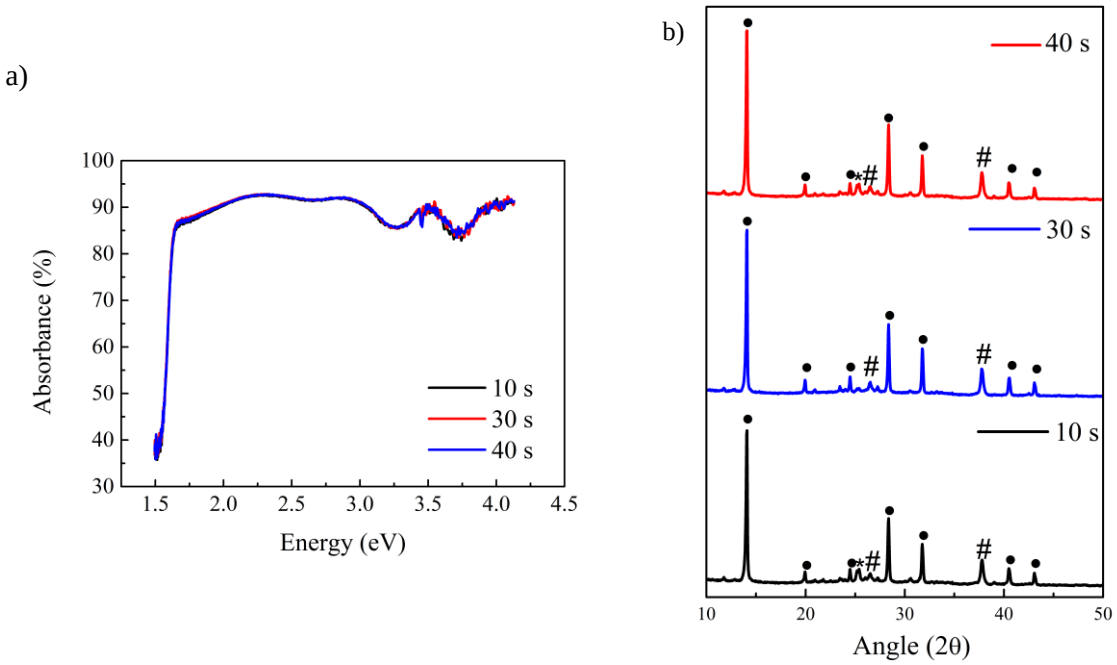

Figure 42 | a) Absorbance and b) XRD for filtered perovskite solution for different perovskite load time: 10 , 30 and 40 s , respectively. The Perovskite layer was deposited as described in Experiemental. For this measurements, CuSCN was not deposited.

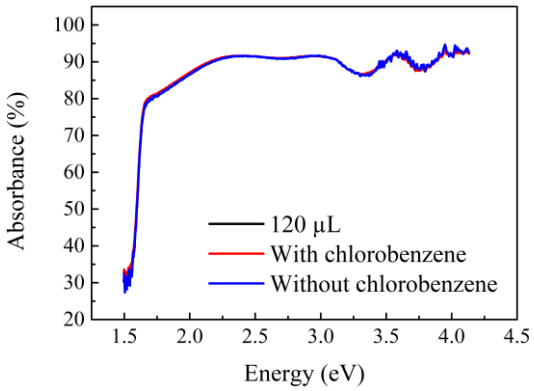

Figure 43 | Absorbance spectra for filtered perovskite solution deposited over c:TiO_2 using TTIP precursor solution, using a mp:TiO_2 and Li^+ doping for different amonts of chlorobenzene: a) 100 µL, b) 120 µL and with chlorobenzene inside spin-coating c). The Perovskite layer was annealed in a tube furnace with an annealing program at RT to 90ºC for 40 min and remaining 15 min. For this measurements, CuSCN was not deposited.

E Electrical characterization

This section presents the *J-V* and *P-V* curves to study the influence of the volume of solution to be dropped for CuSCN (1) and (2), dissolved in di-n-propyl sulfide and dissolved in diethyl sulfide, respectively.

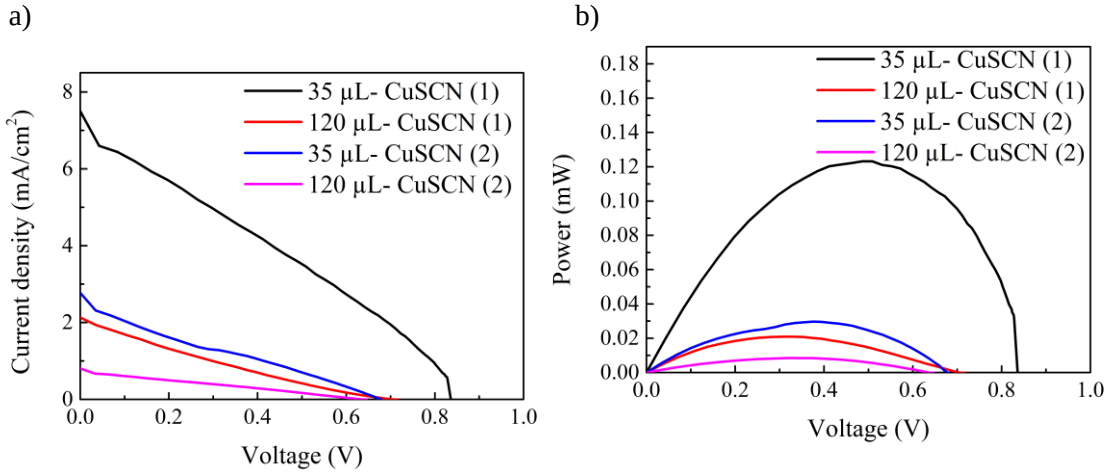

Figure 44 | a) *J-V* and b) *P-V* measurements with the volume of solution for diferent CuSCN (dissolved in di-n-propyl sulfide solution- CuSCN (1) and dissolved in diethyl sulfide- CuSCN (2)). The perovskite solution was deposited over c:TiO_2 using TTIP precursor solution, using a mp:TiO_2 and Li^+ doping. The Perovskite layer was annealed in a tube furnace with an annealing program at RT to 90ºC for 40 min and remaining 15 min.

F Solar cells images

In this section is shown some images of PSCs made during this thesis that are integrated during the text of the section 3.2.5, 3.2.7 and 3.8.2 from Results and Discussion. It is also shown an image about the influence of perovskite film over a compact, mesoporous TiO_2 layer and doped with Li^+.

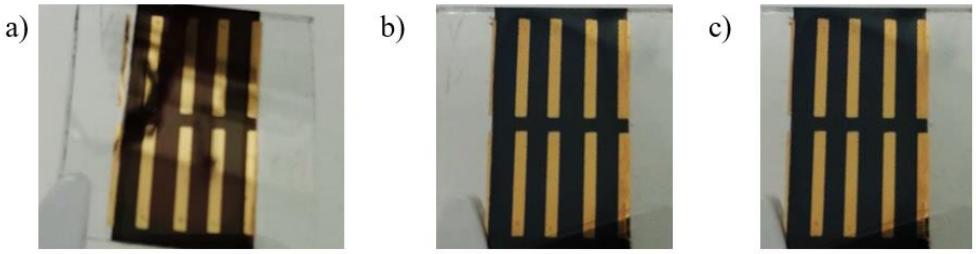

Figure 45 | Solar cells batch of perovskite film deposited over mesoporous TiO_2 layer with a)10 s, b) 30 s and c) 40 s of perovskite load time. CuSCN dissolved in di-n-propyl sulfide.

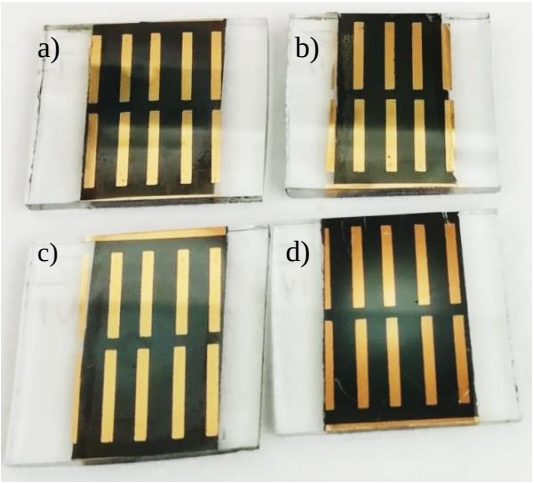

Figure 46 | Solar cells batch of perovskite film deposited over mesoporous TiO_2 layer. a) and b) shows the PSC with filtered CuSCN and c) and d) unfiltered CuSCN dissolved in di-n-propyl sulfide.

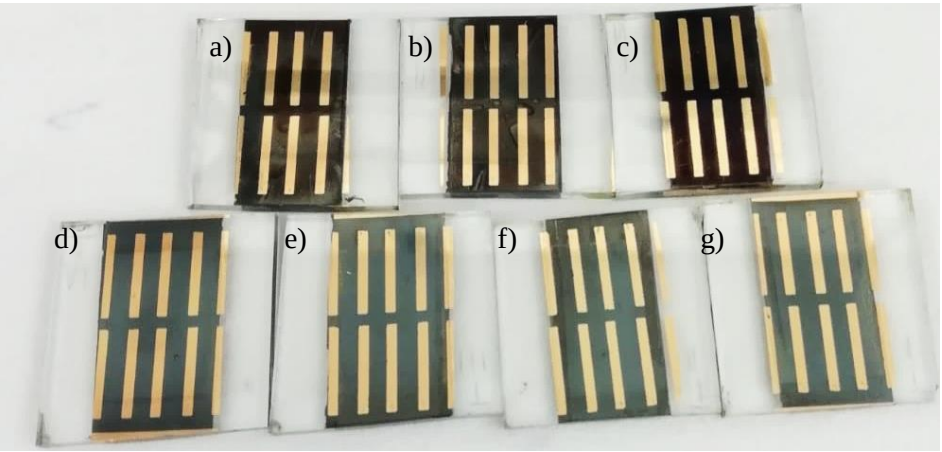

Figure 47 | Solar cell batch of perovskite films deposited over mesoporous TiO_2 layer using a), b) and c) CuSCN dissolved in diethyl sulfide and d), e), f) and g) CuSCN dissolved in di-n-propyl sulfide.